Cargo-selective apical exocytosis in epithelial cells is conducted by Myo5B, Slp4a, Vamp7, and Syntaxin 3

Georg F. Vogel,[1,2] Katharina M.C. Klee,[1,4,5] Andreas R. Janecke,[3] Thomas Müller,[3] Michael W. Hess,[2] and Lukas A. Huber[1]

[1]Division of Cell Biology, Biocenter, [2]Division of Histology and Embryology, and [3]Department of Paediatrics I, Medical University of Innsbruck, 6020 Innsbruck, Austria
[4]Institute of Molecular Biology and [5]Center for Molecular Biosciences Innsbruck, University of Innsbruck, 6020 Innsbruck, Austria

Mutations in the motor protein Myosin Vb (Myo5B) or the soluble NSF attachment protein receptor Syntaxin 3 (Stx3) disturb epithelial polarity and cause microvillus inclusion disease (MVID), a lethal hereditary enteropathy affecting neonates. To understand the molecular mechanism of Myo5B and Stx3 interplay, we used genome editing to introduce a defined Myo5B patient mutation in a human epithelial cell line. Our results demonstrate a selective role of Myo5B and Stx3 for apical cargo exocytosis in polarized epithelial cells. Apical exocytosis of NHE3, CFTR (cystic fibrosis transmembrane conductance regulator), and GLUT5 required an interaction cascade of Rab11, Myo5B, Slp4a, Munc18-2, and Vamp7 with Stx3, which cooperate in the final steps of this selective apical traffic pathway. The brush border enzymes DPPIV and sucrase-isomaltase still correctly localize at the apical plasma membrane independent of this pathway. Hence, our work demonstrates how Myo5B, Stx3, Slp4a, Vamp7, Munc18-2, and Rab8/11 cooperate during selective apical cargo trafficking and exocytosis in epithelial cells and thereby provides further insight into MVID pathophysiology.

Introduction

Epithelia are highly organized tissues that line the inner and outer surfaces of metazoans and fulfill various functions. Polarized epithelial cells form apical and basolateral plasma membrane domains, which are divided by junctional complexes (Apodaca et al., 2012; Rodriguez-Boulan and Macara, 2014; Overeem et al., 2015) and differ in their protein and lipid composition. Certain transporters, ion channels, and enzymes, as well as phosphatidylinositol phosphates (Martin-Belmonte et al., 2007), are specifically enriched in apical or basolateral membranes. This compartmentalization is established and maintained by different proteins that control membrane transport reactions, including Rab small GTPases, motor proteins, and t-SNAREs (Gaisano et al., 1996; Low et al., 1996; Weimbs et al., 1997; Li et al., 2002). The routing of exocytic carrier vesicles toward the apical plasma membrane, membrane tethering, and subsequent fusion is mediated by an evolutionarily conserved cascade of Rab small GTPases, i.e., Rab8 and Rab11 (Bryant et al., 2010; Apodaca et al., 2012; Donovan and Bretscher, 2012; Gálvez-Santisteban et al., 2012). This process is essential to establish homeostasis of polarized epithelial cells and allows them to accomplish their physiological role, e.g., resorption and secretion as executed by the gut mucosa or renal tubule epithelium.

Defects in establishing and/or maintaining epithelial polarity often result in disease. Microvillus inclusion disease (MVID; Cutz et al., 1989) or polycystic kidney disease (Chapin and Caplan, 2010) are prominent examples. MVID is a rare autosomal-recessive enteropathy, manifesting within a few days or several months after birth (early or late onset, respectively). It is characterized by intractable diarrhea leading to life-threatening dehydration and metabolic acidosis (Cutz et al., 1989; Ruemmele et al., 2006). The only treatment available so far is life-long parenteral nutrition or small-bowel transplantation (Ruemmele et al., 2006). The small intestine of MVID patients displays severe villus atrophy. At the subcellular level, the enterocytes show a variable loss of brush border microvilli, subapical accumulation of different kinds of vesicles (including periodic acid–Schiff [PAS]–positive secretory granules; Phillips et al., 2000), and vacuoles lined by microvilli, so-called microvillus inclusions (Cutz et al., 1989).

Previously, we identified mutations in *MYO5B* to be causative for MVID (Müller et al., 2008; Ruemmele et al., 2010) in the majority of sequenced patients (van der Velde et al., 2013). Myosin Vb (Myo5B) is an unconventional actin motor protein capable of both a tethering (Provance et al., 2008) and an active

Correspondence to Lukas A. Huber: lukas.a.huber@i-med.ac.at; or Michael W. Hess: michael.hess@i-med.ac.at

Abbreviations used in this paper: AMIS, apical membrane initiation site; CFTR, cystic fibrosis transmembrane conductance regulator; GAP, GTPase-activating protein; gRNA, guide RNA; GTD, globular tail domain; IF, immunofluorescence; KI, knockin; MVID, microvillus inclusion disease; PAS, periodic acid–Schiff; qRT-PCR, quantitative real-time PCR; SI, sucrase-isomaltase; WB, Western blotting; WT, wild type; ZFN, zinc finger nuclease.

The Rockefeller University Press $30.00
J. Cell Biol. Vol. 211 No. 3 587–604
www.jcb.org/cgi/doi/10.1083/jcb.201506112

walking motion (Schuh, 2011; Holubcová et al., 2013). Myo5B localizes to the apical compartment in polarized epithelial cells and was shown to interact with Rab small GTPases, e.g., Rab8 and Rab11 (Ruemmele et al., 2010; Roland et al., 2011; Khandelwal et al., 2013; Thoeni et al., 2014). Interestingly, Rab8- or Rab11-deficient mice display a similar intestinal phenotype to MVID, although Rab8/11 mutations in MVID patients have not been reported so far (Sato et al., 2007; Sobajima et al., 2014).

Recently, we identified mutations in *STX3*, an apical t-SNARE protein, as cause for a variant form of MVID (Wiegerinck et al., 2014). This finding suggested that Myo5B and Syntaxin 3 (Stx3) may somehow function together in apical vesicle transport. Recent studies have added to the understanding of the molecular mechanism of Myo5B and Rab small GTPase interplay in the context of epithelial polarity and the pathophysiology of MVID (Roland et al., 2011; Knowles et al., 2014; Thoeni et al., 2014). Yet, the exact cascade and the molecular mechanism of apical targeting of exocytic cargo carriers remained unclear.

To address these questions, we used genome editing to generate a CaCo2 model enterocyte cell line harboring an MVID patient mutation (1125G>A). Here, we show that Myo5B selectively transports apical cargo proteins, e.g., sodium/hydrogen-exchanger 3 (NHE3) and cystic fibrosis transmembrane conductance regulator (CFTR), in concert with Rab8, Rab11, synaptotagmin-like protein 4a (Slp4a), and Stx3 for subsequent apical exocytosis. Loss of Myo5B or Stx3 disrupts this selective apical exocytosis, but the brush border enzymes dipeptidyl peptidase IV (DPPIV) and sucrase-isomaltase (SI) appeared generally unaffected and still correctly localized at the apical plasma membrane. Based on these results, we propose that the defects in selective Myo5B/Stx3/Slp4a/Vamp7/Munc18-2–dependent apical cargo transport of epithelial cells account for the clinical hallmark of MVID, the severe diarrhea, and thus provide further insight into MVID pathophysiology.

Results

Targeted mutation of endogenous Myo5B disrupts epithelial polarity and mimics MVID

Research on Myo5B function and MVID pathophysiology has been hampered by the lack of adequate disease models or cell lines. Therefore, we first generated a genetically solid knockin (KI) cell line, mimicking a reported patient stop codon mutation 1125G>A (Ruemmele et al., 2010). We edited the genome of CaCo2, a human enterocyte model cell line, with custom-designed zinc finger nucleases (ZFNs; Fig. 1 A). Introducing the premature stop codon led to Myo5B depletion on protein (Fig. 1 B) and cytoplasmic RNA levels (Fig. 1 C), indicating the degradation of mRNA via the nonsense-mediated decay pathway. This pathway is part of the cellular quality control of gene translation and degrades mRNA containing premature stop codons to prevent translation of the erroneous transcript (Baker and Parker, 2004). Yet, expression levels of the two isoforms, Myo5A and Myo5C, were not altered upon depletion of Myo5B, suggesting that no compensatory regulation was taking place (Fig. 1 C).

To investigate the potential to establish epithelial polarity, wild-type (WT) and Myo5B KI cells were grown on porous filter supports (monolayer, 2D; Thoeni et al., 2014; Wiegerinck et al., 2014) or embedded in extracellular matrix (cysts, 3D; Jaffe et al., 2008; Dukes et al., 2011) to allow full polarization of the cells. In 3D (Fig. 1 D), WT cells fully polarized, and the brush border enzyme DPPIV was transported to the apical surface only. Furthermore, WT cysts developed one single central lumen. In contrast, KI cells showed a significantly decreased ability to properly establish epithelial polarity. DPPIV was not exclusively transported apically at first and only localized to the apical membrane later. Moreover, KI cysts formed multiple disorganized lumina (Fig. 1, D and E). This severe KI phenotype was reverted (Fig. 1 E) by reintroducing WT Myo5B protein.

Electron microscopic analysis of KI monolayers revealed subcellular features phenocopying the hallmarks of MVID (which also were rescued; Fig. S1 A). Brush border microvilli were reduced in number and length (Fig. 1, F and G), and microvillus inclusions occurred regularly (Fig. S1 B). Additionally, vesicles of different shapes and sizes accumulated subapically, sometimes containing PAS-reactive material (Fig. 1 G and Fig S1, B and C), similar to the heterogeneous vesicle clusters known from MVID patients (Iancu et al., 2007).

According to ultrastructure and electron tomography, most of them resembled early or recycling endosomes or exocytic/secretory compartments rather than late endosomes/lysosomes (Fig. S1 D). For their further characterization, we fed WT and KI cells with the fluid phase tracers HRP and colloidal gold conjugated to BSA (BSA-Au). Neither HRP nor BSA-Au was found within the subapical vesicle clusters of KI cells after 2 h of incubation, whereas both tracers readily labeled all compartments of the canonical early endosome–multivesicular body–lysosomal pathway (Fig. S1 E). Therefore, we consider the vesicle accumulations in KI cells as exocytic/secretory and/or recycling endosomal compartments. Collectively, the use of genome editing to deplete Myo5B resulted in a suitable human MVID model cell line that resembles the major phenotypical hallmarks of MVID.

Myo5B and Stx3 participate in the Rab11/8 cascade

Stx3 is part of the Rab11/8 cascade (Gálvez-Santisteban et al., 2012), and mutations in *STX3* also cause MVID (Wiegerinck et al., 2014). Additionally, Myo5B was shown to be the effector of Rab8 and Rab11 (Ruemmele et al., 2010; Roland et al., 2011; Khandelwal et al., 2013; Thoeni et al., 2014). Therefore, we next tested whether Myo5B can be linked mechanistically to the same vesicle tethering and fusion cascade, which requires interaction with Sec15, an essential subunit of the exocyst complex (Jin et al., 2011; Pylypenko et al., 2013), Rab11a, Rab8a, Slp4a, a v-SNARE–like protein, and Stx3. We performed coaffinity purification experiments for CaCo2 cells expressing HA–Strep-Tactin II (HS)–tagged human Rab8a and Rab11a in the active, GTP-locked state (Peränen et al., 1996; Ullrich et al., 1996) as well as the CaCo2-specific WT isoform of Myo5B (Roland et al., 2009). Coaffinity purification is substantially based on the strong affinity of the HS tag on the bait protein to Strep-Tactin on Sepharose beads, which purify the bait proteins and their interaction partners from cellular lysates (Schmidt and Skerra, 2007). Both Rab8a_Q67L (Fig. 2 A) and Rab11a_Q70L (Fig. 2 B) interacted with Sec15, Slpa4, Rab3B, Stx3, and vice versa with Rab11a and Rab8a. These findings confirm that the exocytic Rab11/8 cascade also exists in polarized enterocytes, therefore being most likely a general mechanism of epithelial cells. Interestingly, Myo5B interacted with all members of this cascade (Fig. 2 C), suggesting that it may contribute to cargo trafficking through this pathway.

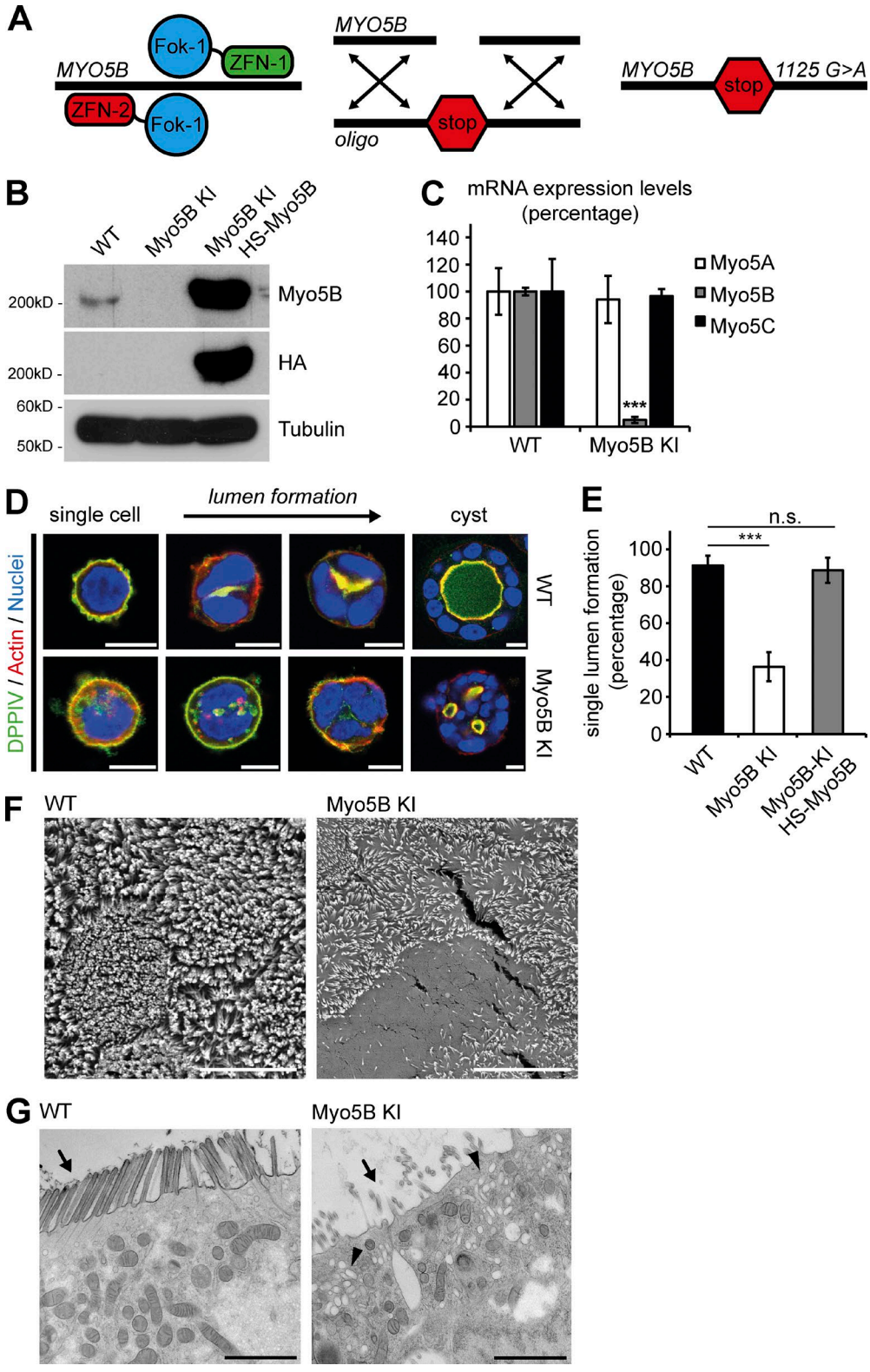

Figure 1. **Generation and characterization of Myo5B KI cells.** (A) Scheme of ZFN-mediated double-strand break and homologous recombination via a short oligonucleotide to introduce the 1125G>A premature stop codon mutation into the CaCo2 genome. (B) Western blot showing Myo5B protein levels of WT, Myo5B KI, and HS-Myo5B–reverted cells. (C) Cytoplasmic mRNA expression levels of Myo5A and Myo5C are not altered upon the depletion of Myo5B. Expression levels were assessed by qRT-PCR. Three independent experiments. (D) Polarity is disrupted upon Myo5B depletion in 3D cyst formation assay in comparison to WT cells (left to right: 24 h, 48 h, 3 d, and 7 d). Bars, 10 µm. (E) Quantification of single lumen formation. $n \geq 100$ cysts/experiment; three independent experiments. (F) Scanning electron micrographs of the apical brush border in 2D CaCo2 cultures. Microvilli of Myo5B KI cells are reduced in size and number. Bars, 5 µm. (G) Transmission electron micrographs of the apical part of CaCo2 show scarce, short microvilli (arrows) and prominent subapical vesicle accumulations (arrowheads) in Myo5B KI cells. Bars, 1 µm. Mean ± SD. ***, $P < 0.005$. n.s., not significant.

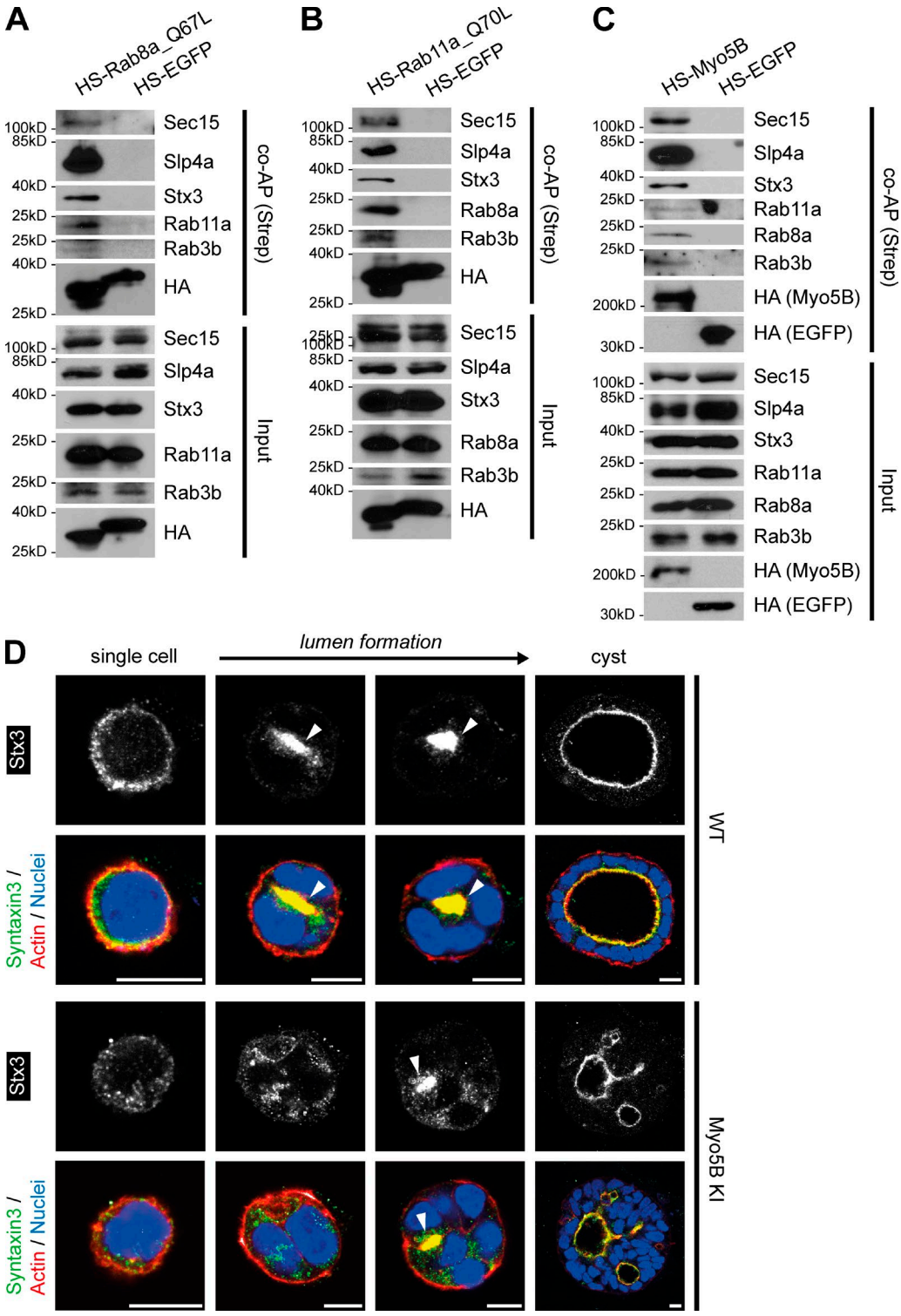

Figure 2. **Analysis of the Rab11/Rab8 cascade in CaCo2.** (A) Rab8a_Q67L interacts with proteins of the apical trafficking route: Sec15, Slp4a, Stx3, Rab11a, and Rab3b. Strep-Tactin was used for coaffinity purification (co-AP). (B) Same as is in A with Rab11a_Q70L as bait and Rab8a interaction. (C) Myo5B interacts with all proteins of the apical trafficking route (compare with A and B). (D) Stx3 localizes correctly during cyst development of Myo5B KI cells despite the overall disrupted polarity (left to right: 24 h, 48 h, 3 d, and 7 d); AMIS is marked by white arrowheads. Bars, 10 µm.

Confocal immunofluorescence (IF) microscopy of polarized monolayers further showed that Rab8a, Rab11a, and Myo5B were observed predominantly at the apical brush border where they colocalized with Stx3, supporting their cooperation in apical exocytosis (Fig. S2). Because Myo5B depletion alters the localization of active Rab8a/11a (Fig. S3, A and B; Knowles et al., 2014), we studied how Myo5B contributes to the subcellular localization of Stx3. In growing WT cysts, Stx3 was mainly found on apical membranes. Despite the severe defects in polarization of, and the formation of multiple lumina

in, growing KI cysts, Stx3 still localized to the apical domains, the apical membrane initiation site (AMIS; Bryant et al., 2010), as well as the brush border (Fig. 2 D). Interestingly, the apical targeting of Stx3 does not require Myo5B and is most likely mediated via *PI45P2* and the transmembrane domain of Stx3 (Gálvez-Santisteban et al., 2012). Based on these results, we conclude that Myo5B functions downstream of, or together with, Stx3 to control the traffic of exocytic cargo to the apical membrane, rather than the identity/compartmentalization and fundamental composition of the apical domain.

Stx3, Rab8a, and Rab11a are essential for epithelial polarity formation

Our results suggest that the motor protein Myo5B might be a possible effector of the Rab11a/Rab8a cascade in collaboration with Stx3 in the exocytosis route of apical cargo (Fig. 2, A–C; Gálvez-Santisteban et al., 2012). Additionally, a time course of developing WT cysts expressing tagged active versions of Rab8a, Rab11a, or Myo5B revealed a partial localization of Rab8a to the AMIS together with Stx3 (Fig. 3 A) and distinct colocalization of Rab11a/Myo5B together with Stx3 on vesicles surrounding the de novo forming apical domain (Fig. 3, B and C). Thus, depletion of these proteins could phenocopy Myo5B deletion. To test this hypothesis, we deleted Stx3 and Rab8a using CRISPR/Cas9-mediated double-strand breaks and depleted Rab11a via RNAi in CaCo2 cells (Fig. S3, C–E). This led to a strongly disturbed polarity phenotype in 3D cysts (Fig. 3, D and E) as reported previously from MDCK cells (Bryant et al., 2010; Gálvez-Santisteban et al., 2012). These phenotypes were fully reverted by reexpression of the respective protein (using expression constructs resistant to the targeting sequences; Fig. 3 E). These results show that Stx3, Rab8, and Rab11 are essential for the establishment of proper epithelial polarity. Together with Myo5B, they collaborate in the targeted transport of vesicles toward the apical plasma membrane.

Differential binding of Myo5B with Rab GTPases defines Stx3 interaction

By introducing specific mutations to Myo5B that selectively affect the binding to Rab8 or Rab11 (Roland et al., 2011), it has been previously demonstrated that apical membrane trafficking in polarized epithelial cells requires Myo5B to interact with Rab8 and Rab11. To mechanistically dissect how Myo5B contributes to cargo exocytosis, we used mutations in the globular tail domain (GTD) of Myo5B (Myo5B-GTD), which selectively affect the binding to Rab8 or Rab11 (Roland et al., 2011). Therefore, we expressed Myo5B_LC (impairs Rab8a binding), Myo5B_ER (disrupts Rab11a binding), or the Myo5B_LC/ER mutant in KI cells. When these mutants were coaffinity purified (Fig. 4 A), it became clear that the binding of Myo5B to Rab11a is crucial for stabilizing the interaction with Sec15. Furthermore, expression of the Myo5B-LC/ER mutant reduced the Stx3 interaction, although in vitro Stx3 and Myo5B-GTD can potentially interact in a direct manner (Fig. S3 F). Microscopy studies also revealed that Rab binding–deficient mutants of Myo5B did not localize strictly to the apical plasma membrane anymore, and concomitantly colocalization with the apical Stx3 was strongly reduced (Fig. S4). These findings imply that Rab11a is essential for a proper recruitment of Myo5B, which appears to be the active motor protein transporting the cargo vesicle to the close proximity of Stx3. Additionally, expression of Myo5B mutants did not prevent the accumulation of subapical vesicles (Fig. 4 B), further emphasizing the importance of regulated Myo5B binding to both Rab8a and Rab11a. In line with these results, the disrupted polarity was not rescued upon reexpression of Rab-binding mutants of Myo5B (Fig. 4 C). These findings suggest that the interaction of Rab11 (and possibly Rab8) with Myo5B-GTD is a prerequisite to mediate the interaction of cargo vesicles with the t-SNARE Stx3 at the apical plasma membrane.

Myo5B depletion disrupts specific v-SNARE–t-SNARE interaction

Next, we tested our hypothesis that Myo5B moves exocytic vesicles toward the proximity of the plasma membrane to allow subsequent fusion. For this, the v-SNARE Vamp3 and v-SNARE–like protein Slp4a—both reported to be involved in apical trafficking (Galli et al., 1998; Gálvez-Santisteban et al., 2012)—and the t-SNARE Stx3 were HS tagged and expressed in CaCo2 WT and KI cells. Coaffinity purification experiments demonstrated that the interaction of Vamp3 with Stx3, Rab11a, and Rab8a remained unaffected by Myo5B depletion (Fig. 5, A, C, and D). In contrast, the interaction of Slp4a with Stx3 required Myo5B (Fig. 5 B). Consistently, Stx3 failed to interact with Sec15, Rab11a, Rab8a, and Rab3b upon depletion of Myo5B (Fig. 5 C). We conclude that Myo5B transports the cargo vesicles loaded with Rab11a, Rab8a, Sec15, and the v-SNARE–like Slp4a toward the apical plasma membrane, where Stx3-mediated vesicle fusion occurs.

Because Slp4a–Stx3 binding has been previously shown to be mediated by the interaction with the Sec1/Munc18-like (SM) protein Munc18-2 (Fukuda et al., 2005), we wondered whether Stx3–Munc18-2 binding was also affected by Myo5B depletion. Indeed, Stx3–Munc18-2 interaction was strongly reduced in Myo5B KI cells (Fig. 5 D). Additionally, we tested the interaction of Stx3 with two other apical v-SNAREs, i.e., Vamp7 and Vamp8 (Pocard et al., 2007; Wang et al., 2007). Myo5B deletion strongly reduced the interaction of Vamp7 with Stx3, but Vamp8–Stx3 binding remained unaffected (Fig. 5 D). Interestingly, Vamp7 interacted with active Rab11a but not with active Rab8a or Myo5B (Fig. 5 E).

To assess whether Myo5B was indeed required for the delivery of apical cargoes in epithelial cells, we used an established model cargo for apical exocytosis. Full-length Influenza A HA (Huber et al., 1993) was expressed in WT and KI cells, and its apical delivery was monitored by confocal fluorescence microscopy. In WT cells, the majority of HA was found at the apical surface. In contrast, upon the deletion of Myo5B, the majority of HA was detected intracellularly, and only a small portion was delivered to the cell surface (Fig. S5 A). Collectively, Myo5B seems crucial for the cognate v- and t-SNARE interaction needed for membrane fusion.

Myo5B and Stx3 conduct selective apical cargo trafficking

We next asked which apical cargo proteins are transported via the Myo5B-, Spl4a-, and Stx3-dependent pathway. Therefore, we determined whether the apical transport of three functionally distinct transmembrane transporters, NHE3 (Yoo et al., 2012; Yang et al., 2015), CFTR (Tang et al., 2011), and glucose transporter 5 (GLUT5; Uldry and Thorens, 2004), required Myo5b. All three are pivotal transporters. NHE3 mislocalizes in MVID patients (Ameen and Salas, 2000), and CFTR in particular was shown to be Myo5B dependent (Swiatecka-Urban et al., 2007). In WT cells, all three transporters localized to the apical surface

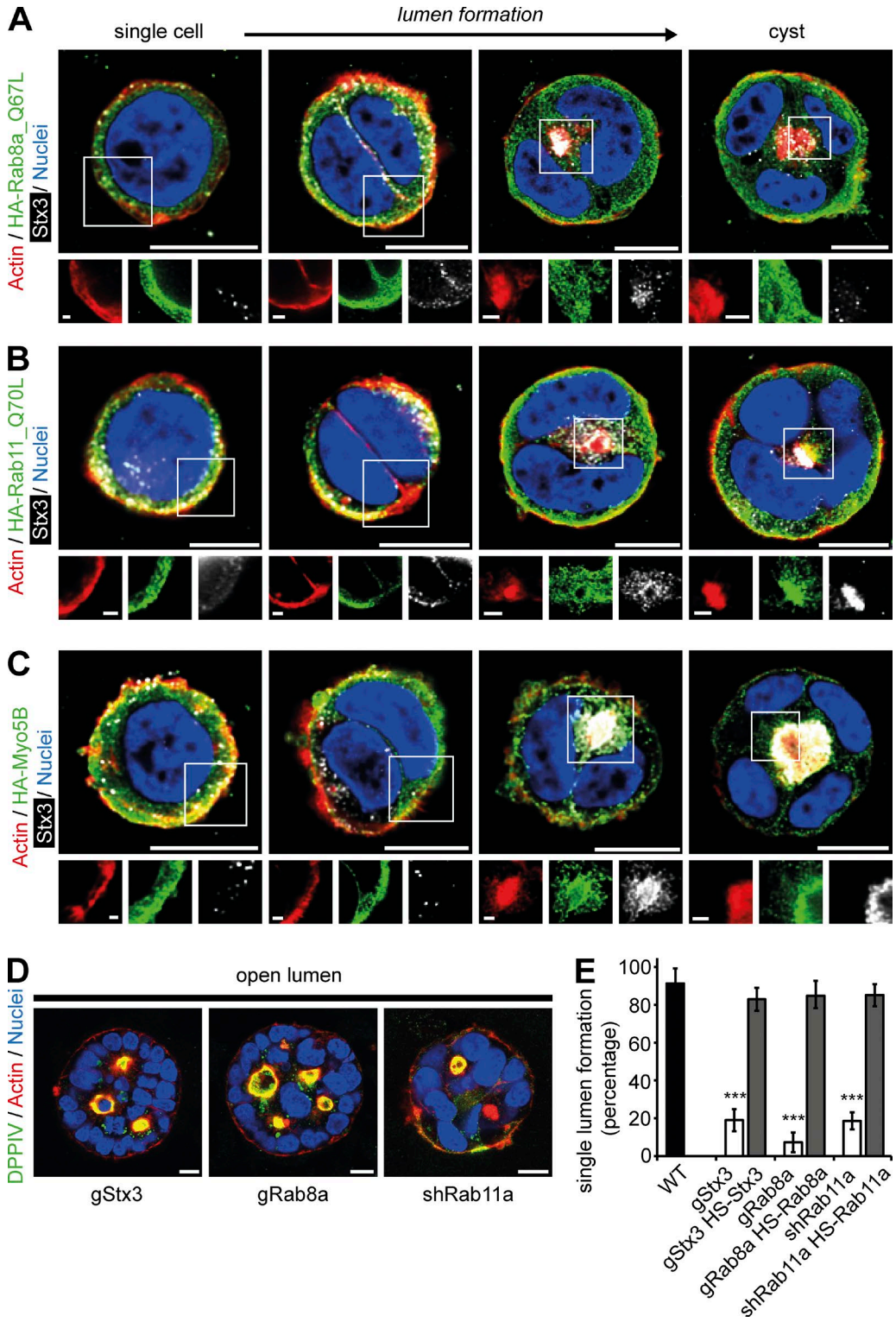

Figure 3. **Stx3, Rab8a, and Rab11a are pivotal for epithelial polarity.** (A) Rab8a_Q67L partly colocalizes with Stx3 at the AMIS (third and fourth columns). (B) Localization of Rab11a_Q70L changes from the periphery to the AMIS, colocalizing with Stx3 as soon as lumen formation starts (third and fourth columns). (C) Myo5B localizes to the periphery (first and second columns) but shows high colocalization with Stx3 at the AMIS (third and fourth columns) when lumen formation begins. (D) Depletion of Stx3 (gSTX3), Rab8a (gRab8a), and Rab11a (shRab11a) results in disrupted cyst polarity (7 d). The apical enzyme DPPIV still localizes correctly (green). (E) Quantification of single lumen formation. Mean ± SD. ***, $P < 0.005$. $n \geq 100$ cysts/experiment; three independent experiments. White boxes in A–C indicate detailed views in separate colors. Bars: (A–C) 10 µm; (magnifications) 1 µm; (D) 10 µm.

of enterocytes. In contrast, upon deletion of Myo5B, NHE3, CFTR, and GLUT5 were no longer found strictly apical, but localized in a more vesicular pattern scattered throughout the cytoplasm (Fig. 6 A and Fig. S5 B). Additionally, NHE3 mislocalized similarly when Stx3 was deleted (Fig. 7 B), but localized apically upon deletion of Vamp3 (Fig. 8 C and Fig. S3 G).

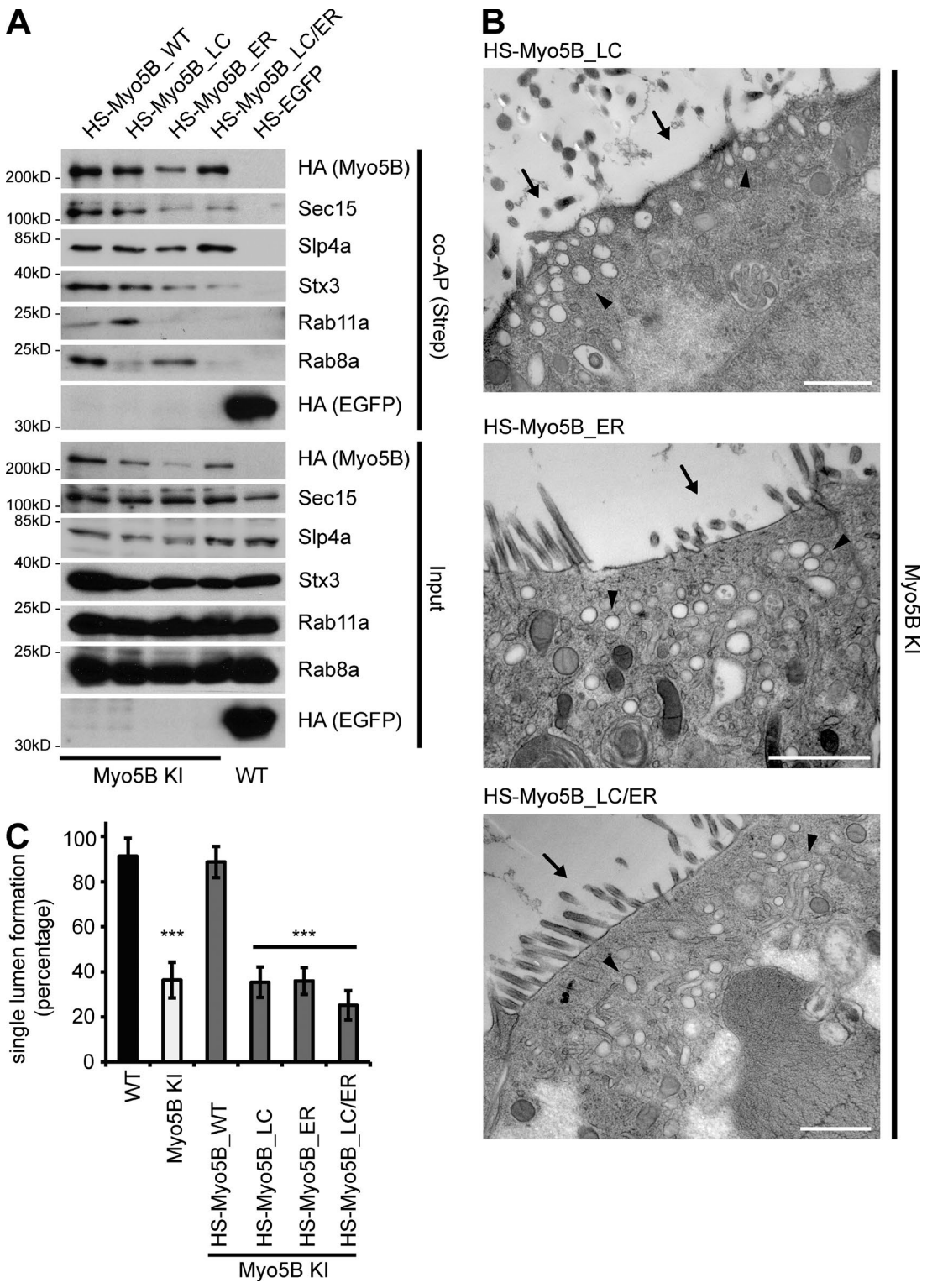

Figure 4. **Rab8a and Rab11a binding of Myo5B is important for its proper function.** (A) Sec15 and Stx3 interaction is reduced in Rab11a and Rab8a/11a binding–deficient mutants of Myo5B. Strep-Tactin was used for coaffinity purification (co-AP). (B) Rab binding–deficient mutants of Myo5B fail to rescue the brush border defects (arrows) and the subapical accumulation of vesicles (arrowheads) in Myo5B-depleted cells. Bars, 1 µm. (C) Quantification of single lumen formation shows that Rab binding–deficient mutants of Myo5B fail to rescue the polarity defect upon Myo5B depletion. Mean ± SD. ***, $P < 0.005$. $n \geq 100$ cysts/experiment; three independent experiments.

Interestingly, the apical brush border enzymes DPPIV (Figs. 1 D, 6 B, and 8 B), aminopeptidase N (Fig. 7 C), and SI (Fig. 8 A) still localized properly at the apical brush border. Previous work suggested that these enzymes are delivered apically via Stx3 (Weisz and Rodriguez-Boulan, 2009). However, upon deletion of Stx3 or overexpression of a dominant-negative Stx3 mutant lacking the transmembrane domain (Stx3_1-247; Wiegerinck et al., 2014), the localization of DPPIV (Figs. 3 D and 7 A)

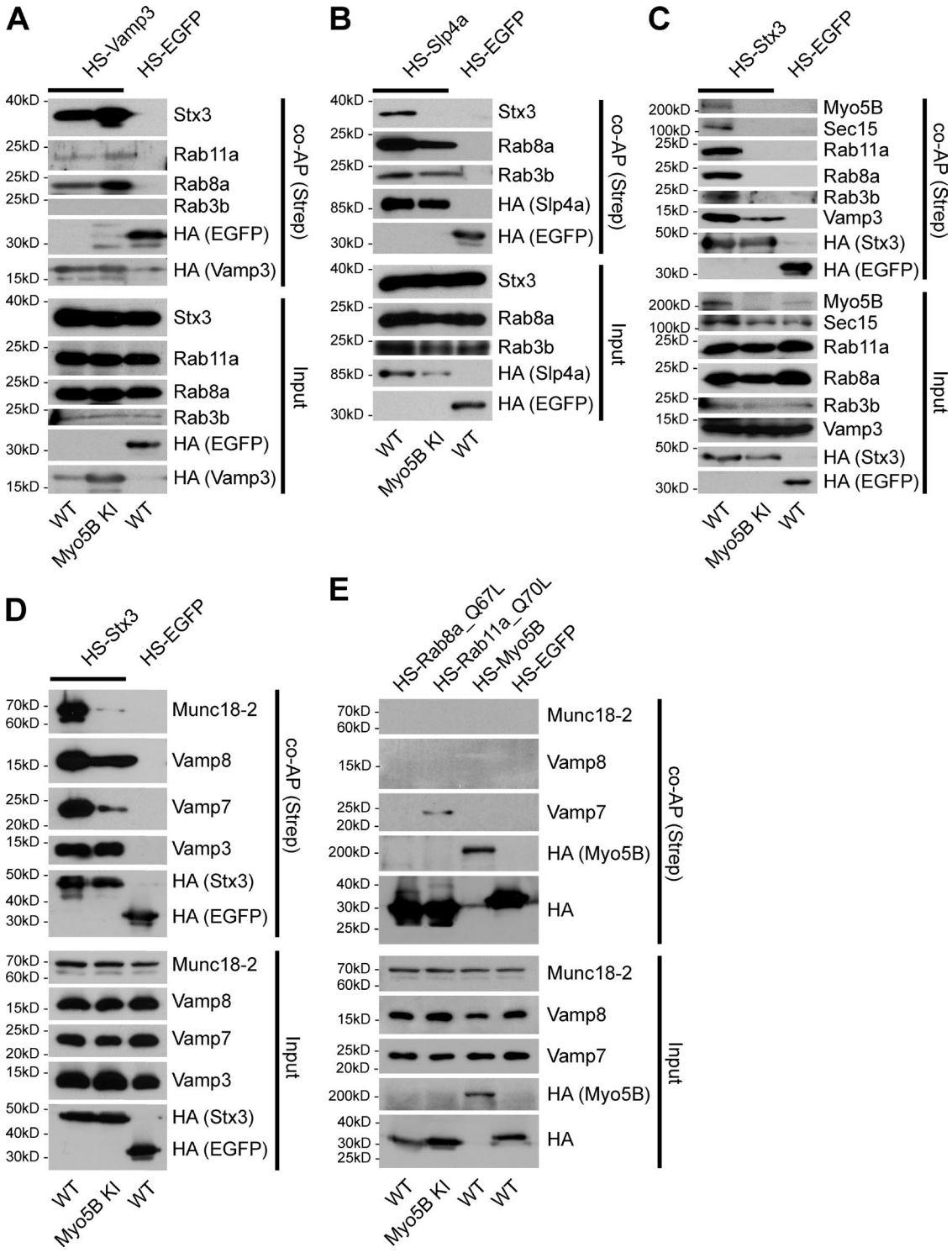

Figure 5. **Myo5B is required for Slp4a–Stx3 interaction.** (A) Interaction between v-SNARE Vamp3, Rab11a, Rab8a, and Rab3b is not affected by Myo5B depletion. (B) Interaction between v-SNARE–like Slp4a and t-SNARE Stx3 is abolished upon Myo5B depletion. The interaction with Rab8a and Rab3b is not affected. (C) v-SNARE Stx3 fails to pull down proteins of the apical cargo trafficking pathway, Sec15, Rab11a, Rab8a, or Rab3b, when Myo5B is deleted. Interaction with t-SNARE Vamp3 remains unaffected (compare with A). (D) Interaction between SM protein Munc18-2 with Stx3 and apical v-SNA RE Vamp7 with Stx3 is strongly reduced upon deletion of Myo5B, whereas Vamp8/Stx3 and Vamp3/Stx3 interaction seems unaffected. (E) Active Rab11a affinity purifies Vamp7 but active Rab8a or Myo5B. Munc18-2 and Vamp8 do not interact with any of the bait proteins. (A–E) Strep-Tactin was used for coaffinity purification (co-AP).

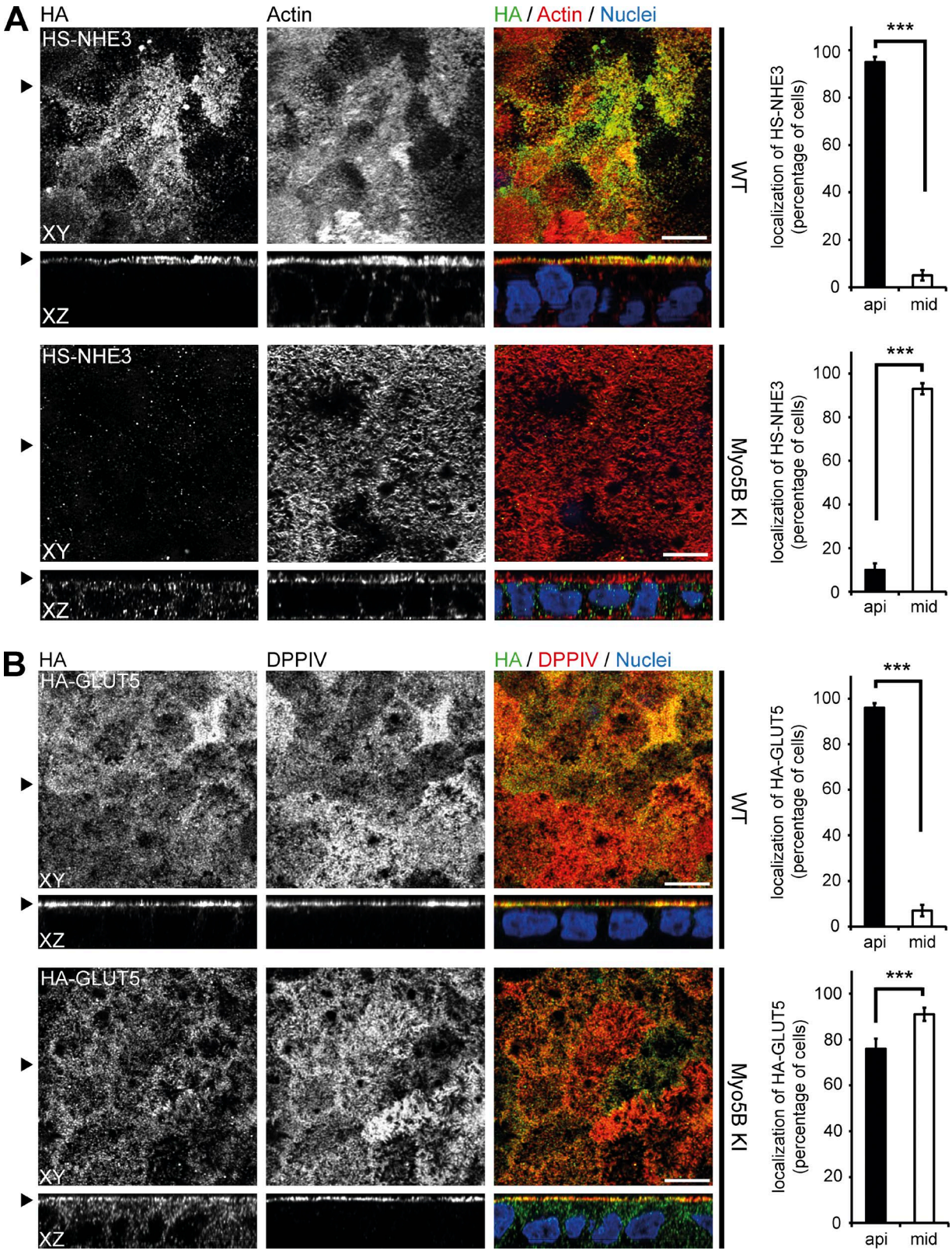

Figure 6. **Myo5B mediates selective cargo transport.** (A) NHE3 resides apically in WT (brush border actin is stained), but mislocalizes throughout the cytoplasm upon Myo5B deletion. Bars, 10 µm. (B) GLUT5 localizes at the apical plasma membrane in WT, but appears dispersed in the cytoplasm upon deletion of Myo5B. DPPIVs apical localization seems unaffected. Arrowheads on the left mark the corresponding XY and XZ planes. Quantification and statistical analysis of indicated cargo/enzyme localization is shown to the right of corresponding confocal micrographs. Bars, 10 µm. Mean ± SD. ***, $P < 0.005$. $n \geq 100$ cells. api, apical/brush border plane; mid, middle/nuclear plane.

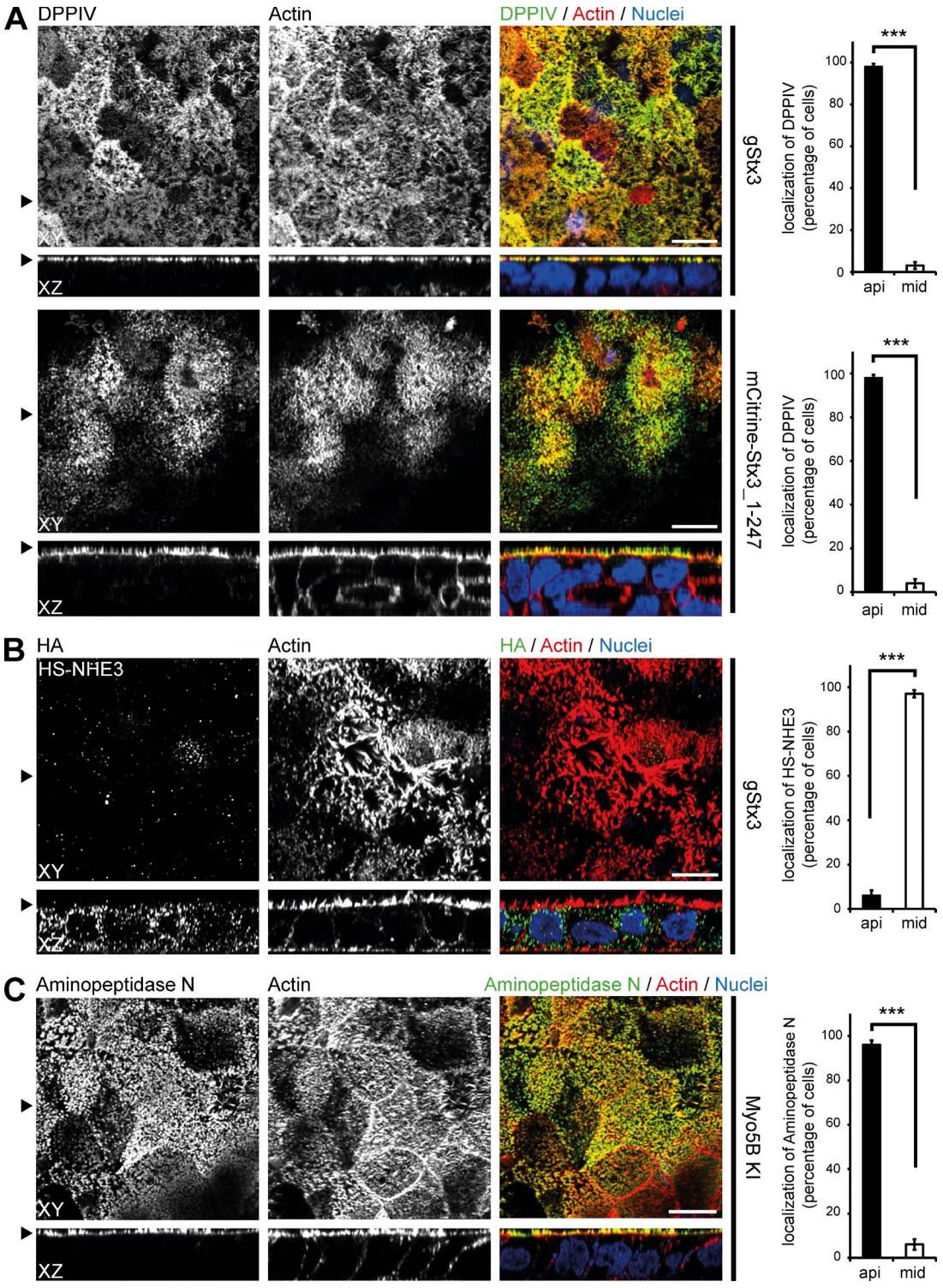

Figure 7. **Myo5B and Stx3 deletion results in selective cargo mislocalization.** (A) Depletion of Stx3 (gStx3) or the expression of a dominant-negative Stx3 (mCitrine-Stx3_1-247) mutant does not affect the correct apical localization of DPPIV. Stx3_1-247 expression results in disrupted polarity (multilayer formation; Wiegerinck et al., 2014). (B) NHE3 is mislocalized from the brush border (highlighted by actin staining) to the cytoplasm in Stx3-depleted cells (gSTX3). (C) Correct localization of aminopeptidase N to the brush border (highlighted by actin staining) upon deletion of Myo5B. Arrowheads on the left mark the corresponding XY and XZ planes. Quantification and statistical analysis of indicated cargo/enzyme localization is shown to the right of corresponding confocal micrographs. Mean ± SD. ***, $P < 0.005$. $n \geq 100$ cells. Bars, 10 µm. api, apical/brush border plane; mid, middle/nuclear plane.

and SI (Fig. 8 A) appeared unchanged in enterocytes. These findings strongly suggest that DPPIV, SI, and aminopeptidase N are transported independently of Myo5B, Slp4a, Vamp3, and Stx3, presumably via an alternative transport route.

Altogether, our results demonstrate that Myo5B, Slp4a, Munc18-2, Vamp7, and Stx3 function together and are thereby involved in selective apical transport of NHE3, CFTR, or GLUT5 in polarized epithelial cells.

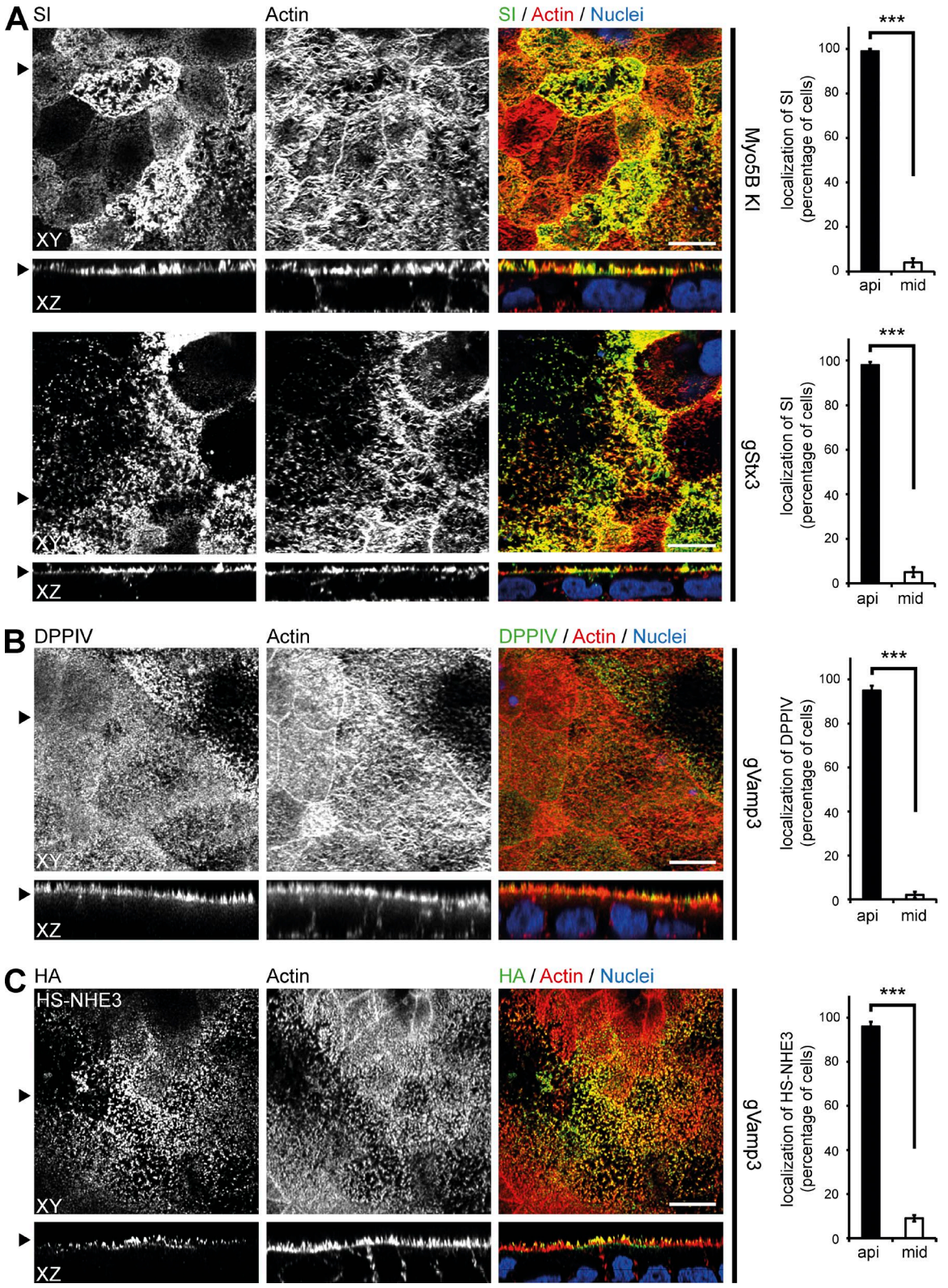

Figure 8. **Deletion of Myo5B and Stx3, but not Vamp3, results in selective cargo mislocalization.** (A) Apical localization of SI seems unaltered upon deletion of Myo5B or Stx3 (gSTX3). (B) Apical localization of DPPIV seems unaltered upon deletion of Vamp3 (gVamp3). (C) Apical localization of HS-NHE3 seems unaltered upon deletion of Vamp3 (gVamp3). Arrowheads on the left mark the corresponding XY and XZ planes. Quantification and statistical analysis of indicated cargo/enzyme localization is shown to the right of corresponding confocal micrographs. Mean ± SD. ***, $P < 0.005$. $n \geq 100$ cells. Bars, 10 µm. api, apical/brush border plane; mid, middle/nuclear plane.

Stx3 interacts with Rab GTPase-activating proteins (GAPs)

In addition to the observed exocytosis defect upon Myo5B deletion, we were interested in the mechanism underlying the termination of the proposed cascade. In *Saccharomyces cerevisiae*, the conserved Rab/Myo5 cascade is terminated at the plasma membrane via the recruitment of a Rab GAP (Donovan and Bretscher, 2012, 2015). We tested whether this also holds true for the cascade of apical cargo exocytosis in polarized epithelial cells. We expressed HS-tagged GAP proteins TBC1D30, a Rab8a GAP, and Evi5, a Rab11a GAP. Both GAPs are known to regulate their respective Rab GTPases in the context of epithelial polarity (Yoshimura et al., 2007; Bryant et al., 2010; Westlake et al., 2011; Apodaca et al., 2012; Lim and Tang, 2013). Pull-down experiments revealed that both GAPs interacted with Stx3, Myo5B, and Slp4a (Fig. 9 A). However, only TBC1D30 coaffinity purified Sec15 (Fig. 9 A). To further evaluate the interaction, Stx3, TBC1D30, Evi5, and Snap23a as a positive control (Galli et al., 1998) were expressed in *Escherichia coli* and purified. Indeed, both TBC1D30 and Evi5 interacted in a direct manner with Stx3 (Fig. 9, B–D), indicating that Stx3 recruits the Rab GAP proteins to the apical plasma membrane. To test this hypothesis, we compared the localization of both GAPs in CaCo2 WT and Stx3-depleted cells. In WT cells, Evi5 was found at the apical plasma membrane but was more dispersed in the cytoplasm in the absence of Stx3 (Fig. 9 E). Interestingly, the distribution of TBC1D30 seemed mostly unaffected upon the deletion of Stx3 (not depicted). This could be the result of other (to us unknown) interaction partners.

Collectively, these data show that the Rab8/11 GAPs interact with Stx3 at the apical plasma membrane. At this state, the cargo vesicle is presumably tethered to the plasma membrane via the exocyst complex and undergoes fusion via v-SNARE–t-SNARE interaction, as exemplified by Sec15–Slp4a interaction with the GAP proteins (Fig. 9 A and Fig. 10, A and C).

Discussion

Exocytosis in polarized epithelial cells is a highly orchestrated process. Several players, such as Rab small GTPases, motor proteins, or fusion factors, are required for transporting cargo molecules through vesicular carriers toward either of the two plasma membrane domains. Defects in these processes often interfere with epithelial polarity and result in disease. Mutations in both the motor protein Myo5B and the t-SNARE Stx3 were shown to cause MVID in infants (Müller et al., 2008; Ruemmele et al., 2010; Wiegerinck et al., 2014). Because of the rareness of MVID, research has been mostly performed in ex vivo cell cultures through use of conventional RNAi approaches (Ruemmele et al., 2010; Knowles et al., 2014; Thoeni et al., 2014). Here, we studied the function of Myo5B and its role in epithelial trafficking and exocytosis by using a human cell model that carries the 1125G>A MVID patient mutation. This approach allowed us to further dissect the reported Rab11/Rab8 cascade (Gálvez-Santisteban et al., 2012) and to establish Myo5B as the motor for selective cargo transport in dependence of Slp4a and Stx3. Additionally, we could show that the interaction between Myo5B and Stx3 relies on the recruitment of Myo5B by Rab11a. As the second Rab11 isoform Rab11b has a distinct function independent of Rab11a (Lapierre et al., 2003), we focused on Rab11a and its established function in epithelial cells in this study.

Recent publications on Rab11a knockout mice have shown NHE3 mislocalization and MVID-like ultrastructural features (Sobajima et al., 2014; Knowles et al., 2015), further strengthening our model of selective cargo transport (Fig. 10, A–D): apically destined cargo, such as NHE3, CFTR, or GLUT5, are transported via Rab11a/Rab8a and Myo5B toward the vicinity of the apical plasma membrane, where the exocyst tethers cargo vesicles and, subsequently, the v-SNARE–like Slp4a and the apical t-SNARE Stx3 mediate vesicle fusion. Conceivably, the interaction of Stx3 and the Rab GAPs TBC1D30 and Evi5 could then terminate the association of Rab GTPases and Myo5B from the vesicle's membrane at the apical plasma membrane to allow the Rab GTPases to recycle back into the cytoplasm (Fig. 10 C). Interestingly, this could imply that t-SNAREs serve as hubs to terminate several distinct incoming exocytosis routes. Especially regarding MVID, loss-of-function mutations or deletion of Myo5B, Stx3, or any other of the components involved prevent proper targeting (Fig. 10 B) and most likely result in subapical accumulation of cargo vesicles as seen in electron micrographs of patients and cell models. Only recently, the first two Myo5B knockout mouse models were published (Cartón-García et al., 2015; Schneeberger et al., 2015). These new models will be an adequate tool to further understand MVID, as both recapitulate MVID symptoms.

Based on a thorough dissection of the apical exocytosis route that requires Myo5B, Rab11a, Rab8a, Slp4a, Vamp7, Munc18-2, and Stx3, we provide additional insight into MVID pathophysiology. NHE3 is essential for intestinal sodium homeostasis, and NHE3 knockout mice suffer from intractable diarrhea (Larmonier et al., 2013). Furthermore, NHE3 mislocalization was also reported from MVID (Ameen and Salas, 2000). Conceivably, upon disruption of the exocytosis cascade, NHE3 mislocalization could partially account for increased sodium loss in stools from MVID patients (Salomon et al., 2014). Furthermore, GLUT5 mislocalization likely contributes to intestinal malabsorption.

Decreased DDPIV and SI immunolabeling generally accompanies intestinal brush border atrophy. A few MVID cases and Rab8 and Rab11 knockout mice showed more intracellular enrichment of these enzymes (Ameen and Salas, 2000; Reinshagen et al., 2002; Sato et al., 2007; Knowles et al., 2014; Sobajima et al., 2014), opposing the apparently normal distribution of DPPIV/SI in our KI/mutant cell lines. Other work on MVID patient biopsies, however, revealed an intact biosynthetic pathway and exocytosis of DPPIV/SI (Phillips et al., 1993). Because our cell lines carry specific Myo5B and STX3 mutations, they allowed us to detect the selective cargo transport routes described here. However, they certainly do not reflect the whole variability of MVID (Iancu et al., 2007) caused by mutations of *MYO5B*, *STX3*, and possibly other still unknown genes.

How and why epithelial cells accomplish selective apical cargo transport remains unsolved. Apically destined cargo is shuttled via the Golgi apparatus and trans-Golgi network toward the plasma membrane. Presumably, signals defining the trafficking pathway, e.g., Rab GTPases, motor proteins, and finally v-/t-SNARE couplings, are encoded on the cargo proteins. NHE3, CFTR, and GLUT5, for example, are proteins containing several transmembrane helices. Furthermore, NHE3 (Weinman et al., 2003) and CFTR (Moyer et al., 1999) contain PDZ motifs at the C-terminal end, which GLUT5 does not. However, DPPIV, SI, and aminopeptidase N are heavily glycosylated proteins with a single transmembrane span, but not glycophosphatidylinositol anchored (Paulick and Bertozzi,

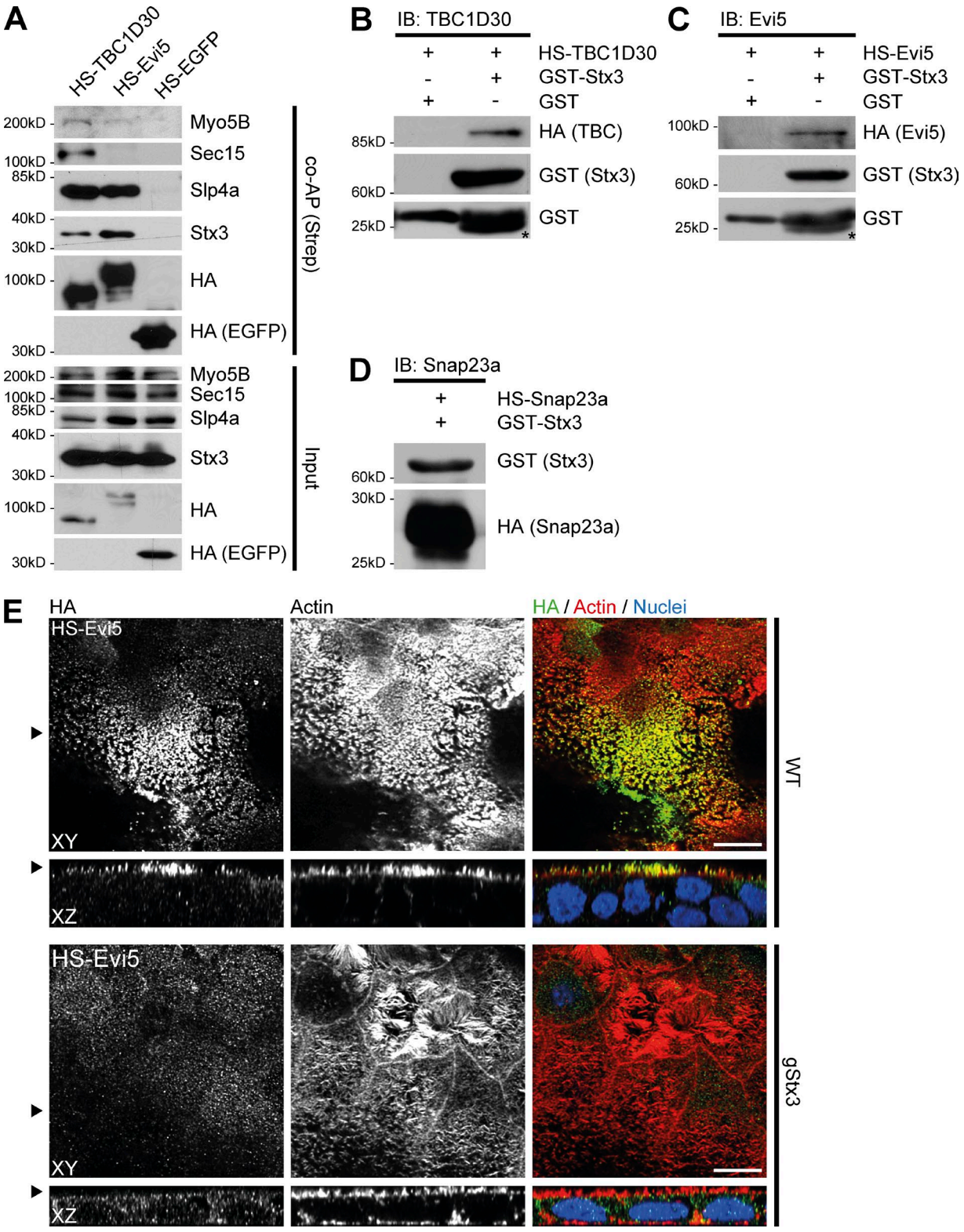

Figure 9. **Rab8a/Rab11a GAPs interact with Stx3.** (A) TBC1D30 and Evi5 interact with Stx3 and partially with proteins of apical cargo trafficking in CaCo2 cells. Strep-Tactin was used for coaffinity purification (co-AP). (B) TBC1D30 and Stx3 interact directly in vitro. GST alone was used as a negative control. (C) Evi5 and Stx3 interact directly in vitro. GST alone was used as a negative control. The asterisk indicates the GST degradation background band. (D) In vitro interaction of Snap23a and Stx3 was used as a positive control for B and C. (E) Evi5 localizes at the apical plasma membrane in WT but appears dispersed in the cytoplasm upon deletion of Stx3 (gStx3). Arrowheads on the left mark the corresponding XY and XZ planes. Bars, 10 µm. IB, immunoblotting.

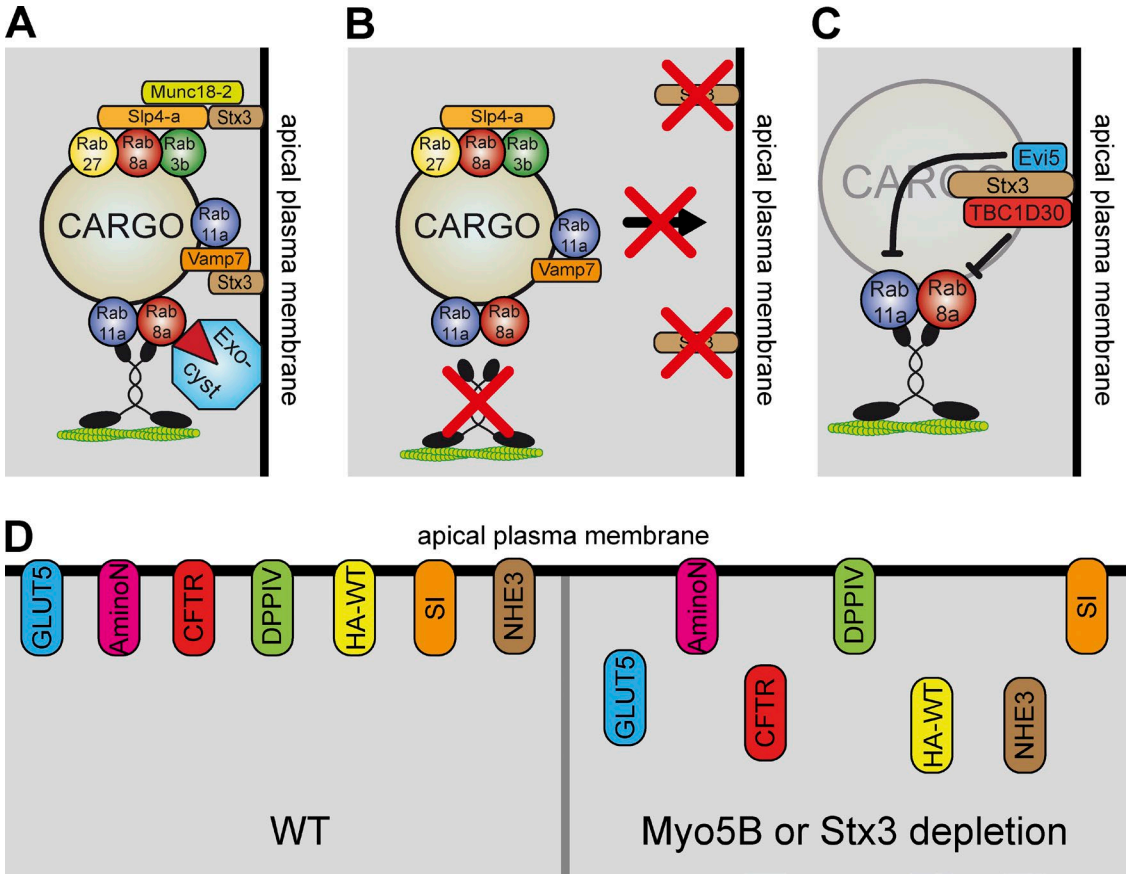

Figure 10. **Schematic summary.** (A) Cargo vesicles are delivered to the apical plasma membrane in dependence on Rab11a, Rab8a, and Myo5B. The v-SNARE–like Slp4a is recruited to the vesicle via Rab27, Rab8a, and Rab3b and binds the t-SNARE Stx3 together with the SM protein Munc18-2 to allow the vesicle to fuse with the plasma membrane. The v-SNARE Vamp7 interacts with Rab11a and Stx3. (B) Upon depletion of either Myo5B or Stx3, cargo vesicles are no longer delivered properly. (C) Apical cargo transport is most likely terminated via the Rab GAPs TBC1D30 and Evi5, which interact with Stx3 at the apical plasma membrane and catalyze the transition to the inactive state of Rab8a and Rab11a. (D) Overview of apical cargo proteins in WT and mislocalization upon depletion of Myo5B or Stx3.

2008). Yet, no commonalities possibly explaining the observed routing of these proteins seem obvious. Conceivably, DPPIV, SI, and aminopeptidase N might be transported to the apical plasma membrane on an alternative route that bypasses the apical recycling endosome. Thus, this route does not depend on the cascade presented here and uses different v-/t-SNARE couplings. Hence, further investigations are necessary for fully understanding the variety of selective cargo transport routes based on distinct cargo and v-/t-SNARE couplings.

Materials and methods

Antibodies and reagents

Primary antibodies directed against Rab8a (Western blotting [WB], 1:1,000; AT3535a; Abgent), Rab11a (WB, 1:1,000; ab128913; Abcam), Rab3b (WB, 1:1,000; 3F12; Abnova), Slp4a (WB, 1:500; HPA001475; Sigma-Aldrich), Sec15 (WB, 1:1,000; ED2003; Kerafast), Stx3 (WB, 1:1,000; IF, 1:100; 133750; Abcam), GST (WB, 1:5,000; Pharmacia), Vamp3 (WB, 1:500; NB300-510; Novus Biologicals), Vamp7 (WB, 1:1,000; ab36195; Abcam), Vamp8 (WB, 1:1,000; ab76021; Abcam), Munc18-2 (WB, 1:1,000; ab103976; Abcam), HA (WB, 1:1,000; IF, 1:500; MMS-101R; Covance), and HA (WB, 1:1,000; IF, 1:500; C29F4; Cell Signaling Technology) are commercially available. Myo5B antibody was described previously (Ruemmele et al., 2010). Primary α-tubulin (WB, 1:1,000; 12G10), DPPIV (IF, 1:100; HBB3/775/42), SI (IF, 1:100; HBB2/614/88), and aminopeptidase N (IF, 1:50; HBB2/614/88) were acquired from the Developmental Studies Hybridoma Bank. Secondary HRP-conjugated goat anti–mouse and goat anti–rabbit (1:5,000; Sigma-Aldrich) were used for WB. Actin filaments were labeled with phalloidin–Alexa Fluor 568 (1:500; Life Technologies). HRP (Sigma-Aldrich) and 5-nm BSA-Au (University Medical Center Utrecht) were used for fluid phase endocytosis. Secondary Alexa Fluor–conjugated (Alexa Fluor 488, 568, and 647) goat anti–mouse (1:1,000; Life Technologies), goat anti–rabbit (1:1,000; Life Technologies), and Hoechst 3342 (1:10,000; Thermo Fisher Scientific) were used for IF labeling.

Genome editing

Custom ZFNs targeting the MYO5B locus were purchased from Sigma-Aldrich. EGFP and E2-crimson were cut out from parental plasmids (a gift from M. Frödin, University of Copenhagen, Copenhagen, Denmark; Duda et al., 2014) and ligated into the ZFN backbones. Single-stranded oligonucleotides (Chen et al., 2011) were used for homologous recombination introducing the 1125G>A point mutation (Ruemmele et al., 2010). Screening for recombination events was done using single cell clones, PCR amplification (forward primer 5′-CCT

CCTGAACCTATCTCCCC-3′ and reverse primer 5′-CCCAGGTA GCAGATAGAGCG-3′), and restriction enzyme digest with BtsI (New England Biolabs, Inc.), which was introduced via homologous recombination. Positive clones were expanded and genomic DNA was purified, PCR amplified, subjected to blunt end TOPO cloning (Invitrogen), and sent for Sanger sequencing. Sequence-verified clones were further tested for Myo5B protein and RNA expression. The highest (score of likelihood) eight predicted off-target hits (National Center for Biotechnology Information; basic local alignment search tool) were tested by Sanger sequencing and resulted as nottargeted/unaffected.

For CRISPR/Cas9-mediated depletion, guide RNA (gRNA) targeting sequences for Rab8a (5′-GAACTGGATTCGCAACATTG-3′), Vamp3 (5′-AAGTCTTCGATTACTGCCAG-3′), and Stx3 (5′-TGA GATTGCTATCGACAACA-3′) were selected using an online prediction tool (CRISPR Design; Zhang lab, Massachusetts Institute of Technology; Hsu et al., 2013). gRNAs were cloned into a lentiCRISPRv2 vector via BsmBI restriction enzyme sites. lentiCRISPRv2 was a gift from F. Zhang (Massachusetts Institute of Technology, Cambridge, MA; Addgene plasmid 52961; Sanjana et al., 2014). Lentiviral transduction was performed as described in the following paragraph. Depletion efficiency was verified via WB, and a gRNA-resistant cDNA was used for rescue experiments.

Plasmids and lentivirus production

Human Myo5B, Rab8a, Rab11a, Stx3, Evi5, TBC1D30 (a gift from J. Peränen, University of Helsinki, Helsinki, Finland), Snap23a, Slp4a, and Vamp3 were amplified via PCR from cDNA/plasmids and ligated into a pENTR-HS vector (a gift from S. Geley, Innsbruck Medical University, Innsbruck, Austria). HA (Huber et al., 1993) was cloned into a pENTR207 (Invitrogen) vector. Point mutations were introduced via PCR-based site-directed mutagenesis (Rab8a_Q67L, Rab11a_Q70L, Myo5B_Q1300L/Y1307C, Myo5B_Y1714E/Q1748R, and Myo5B_ Q1300L/Y1307C/Y1714E/Q1748R). For lentiviral transduction, cDNA was further subcloned via LR clonase into a pCCL-EF1α-BlastiR-DEST lentiviral vector using Gateway Cloning Technology (Invitrogen). mCitrine-Stx3_1-247 has been described previously (Wiegerinck et al., 2014).

shRNA sequence targeting Rab11a (5′-GTCCATTTCCCAG GTCTGAGATTTA-3′) was cloned into a pENTR-THT3 vector using BglII and HindIII sites. Sequence-verified plasmids were used to subclone via LR clonase into either pHR-SFFV-Neo-DEST or pGLTR-X-Puro-DEST (a gift from S. Geley) lentiviral shRNA expression plasmids (Sigl et al., 2014).

Lentiviral plasmids were cotransfected with Lipofectamine LTX (Invitrogen) together with pVSV-G and psPAX2 in the Hek293LTV producer cell line. Viral supernatant was harvested 48 and 72 h after transfection and directly used for CaCo2 cell infection. 6 d after infection, cells were selected with 10 µg/ml puromycin (Sigma-Aldrich) or 20 µg/ml blasticidin S (Invitrogen).

Cell culture

Hek293LTV, CaCo2 WT, and KI cells were cultured in DMEM (Sigma-Aldrich) containing high glucose, sodium pyruvate, 100 U/ml penicillin (Sigma-Aldrich), 100 µg/ml streptomycin (Sigma-Aldrich), 5% nonessential amino acids (Gibco), and 10% FBS (Gibco) in a humidified atmosphere with 5% CO_2 at 37°C. For experiments requiring fully polarized growth conditions, CaCo2 cells were seeded on 24-mm or 75-mm filters (Costar Transwell; pore size of 0.4 µm; Corning) and cultured for 14–28 d.

Quantitative real-time PCR (qRT-PCR)

Cytoplasmic RNA was isolated using an RNeasy Mini kit (QIAGEN). cDNA was transcribed with specific primers and the First Strand cDNA Synthesis kit (Thermo Fisher Scientific). qRT-PCR was performed with a SYBR green qPCR kit (DyNamo ColorFlash; Thermo Fisher Scientific) and the following primers: Myo5A forward (5′-TGA ACGAAATCAGTCCATCATCG-3′) and reverse (5′-CGGCTGCT ATTATCATTCCTGGT-3′), Myo5B forward (5′-TCCCTGACCCTGA TGAGGTAT-3′) and reverse (5′-GACTCCAGGAAACGGACCTT-3′) Myo5C forward (5′-ACACGCAGTACAACAGGGTC-3′) and reverse (5′-GATGTCAGGATTCCGAAGTGG-3′), and GAPDH forward (5′-CGGAGTCAACGGATTTGGTCGTAT-3′) and reverse (5′-AGC CTTCTCCATGGTGGTGAAGAC-3′).

Coaffinity purification assays and WB

For coaffinity purification of HS-tagged proteins, Strep-Tactin purification was performed as described previously (Glatter et al., 2009). In brief, polarized CaCo2 cells were scraped and lysed in NP-40–containing lysis buffer. After separation of nuclei/DNA, lysates were passed by Strep-Tactin resin (IBA Bio TAGnology) in columns (MoBiTec Molecular). Affinity-captured proteins were washed and eluted with biotin (Glatter et al., 2009). CaCo2 cells expressing HS-EGFP were used as a control. WB was performed essentially as described previously (Fialka et al., 1997). Polyvinylidene fluoride membranes were incubated with primary antibody at room temperature for 1 h or overnight at 4°C. Secondary antibody incubation was performed for 1 h at room temperature. Chemiluminescence was exposed on films.

IF microscopy

IF labeling of CaCo2 cells grown on Transwell filters was performed essentially as described previously (Wiegerinck et al., 2014). 3D cyst cultures were processed as previously described (Jaffe et al., 2008), mounted in mowiol. Samples were analyzed at room temperature with an epifluorescent microscope (Axio Imager M1; Carl Zeiss) equipped with a charge-coupled device camera (SPOT Xplorer; Visitron Systems) and recorded with VisiView 2.0.3 (Visitron Systems). Objective lenses used were a 25× oil immersion objective (numerical aperture of 0.8) and a 10× air objective (numerical aperture of 0.3; Carl Zeiss). Single confocal planes or stacks were recorded with a confocal fluorescence microscope (SP5; Leica) using a glycerol 63× lens with a numerical aperture of 1.3 (Leica) at room temperature and mounted in mowiol. The recording software used was LASAF 2.7.3 (Leica). Images were deconvolved with Huygens Professional Deconvolution and Analysis Software (Scientific Volume Imaging), exported using Imaris 3D rendering (Bitplane), and adjusted for brightness, contrast, and pixel size.

In vitro interaction studies

Stx3 and HS-tagged Evi5, TBC1D30, and Snap23a were cloned into a pENTR221 backbone separated by a ribosomal binding site for bicistronic expression in *E. coli* by BP clonase (Invitrogen). Negative controls were constructed the same way, but with a stop codon instead of Stx3. The resulting pENTR221 vectors were subcloned via an LR clonase reaction into a pGEX-3P-DEST vector, which results in the addition of an N-terminal GST tag to the Stx3 reading frame. Myo5B-GTD was amplified by PCR (amino acids 1,237–1,823) and subcloned into a pENTR-HS vector via EcoRV and XbaI restriction enzyme sites. HS–Myo5B-GTD and HS-Stx3 were shuttled to a pDEST17 (Invitrogen) or pGEX-3P-DEST vector, respectively, via LR clonase. GST alone (pGEX-GST) was used as a negative control. Recombinant proteins were expressed in *E. coli* BL21 (DE3), and purification was performed as previously described (Adell et al., 2014). GST-tagged proteins were purified with glutathione–Sepharose 4B (GE Healthcare), washed, and eluated with glutathione. HS-Stx3 was cleaved off from GST immobilized on beads with PreScission protease (GE Healthcare) following the provided instructions. Eluates were subjected to SDS gel electrophoresis, Coomassie stained, or analyzed via WB.

Electron microscopy

Transmission electron microscopy was performed as described previously (Ruemmele et al., 2010; Vogel et al., 2015). In brief, 2D cultures were cryofixed, freeze substituted, and embedded in plastic (Ruemmele et al., 2010). PAS-cytochemistry was performed on thin sections (Ruemmele et al., 2010); DAB cytochemistry for detecting HRP was performed after rehydration of freeze-substituted samples (Vogel et al., 2015). Scanning electron microscopy was performed as described previously (Ruemmele et al., 2010). Transmission electron tomography of 300-nm-thick sections was performed as described previously (Vogel et al., 2015). Dual axis tilt series were recorded on a transmission electron microscope (Tecnai-T20 G2; FEI) with 200 kV at 14,500× magnification from a negative to positive tilt angle of −65–65° (1° increment), with a 4,096 × 4,096–pixel digital camera at a binning of 2 (Eagle; FEI) and with Inspect3D software (FEI). Tomograms were reconstructed and modeled using IMOD software (University of Colorado, Boulder, CO; Kremer et al., 1996; Vogel et al., 2015).

Software and statistics

The software used, if not already specified, were GIMP version 2.8.10 (GNU Image Manipulation Program; open source), ImageJ version 1.49a (National Institutes of Health), Photoshop CS6 (Adobe), Illustrator CS6 (Adobe), and iTEM-analySIS five (Olympus).

Cyst quantification represents the mean of $n \geq 100$ cysts per experiment of at least three independent experiments, error bars represent the SD, and significances were analyzed applying Student's *t* test, unpaired and two-tailed. *, $P < 0.05$; **, $P < 0.01$; ***, $P < 0.005$.

Online supplemental material

Fig. S1 shows further characterization of Myo5B KI cells. Fig. S2 shows colocalization of active Rab8a, 11a, and Myo5B with Stx3 at the apical plasma membrane. Fig. S3 depicts altered localization of active Rab8a and Rab11a upon deletion of Myo5B, as well as depletion efficiency for Stx3, Rab8a, Rab11a, and Vamp3. Fig. S4 shows localization studies of Rab binding–deficient Myo5B mutants. Fig. S5 exhibits altered localization of HA and CFTR upon deletion of Myo5B. Online supplemental material is available at http://www.jcb.org/cgi/content/full/jcb.201506112/DC1. Additional data are available in the JCB DataViewer at http://dx.doi.org/10.1083/jcb.201506112.dv.

Acknowledgments

We thank Angelika Flörl, Karin Gutleben, and Barbara Witting for technical support. Furthermore, we acknowledge Dr. Stephan Geley for providing several plasmids, Dr. Morten Frödin for fluorescent ZFN backbones, Dr. Johan Peränen for TBC1D30 cDNA, and Dr. David Teis as well as Dr. Reinhard Fässler for carefully reading the manuscript.

The Austrian Science Fund within the SFB021 special research program and the Molecular Cell Biology and Oncology PhD program at the Innsbruck Medical University supported this work.

The authors declare no competing financial interests.

Submitted: 23 June 2015
Accepted: 30 September 2015

References

Adell, M.A., G.F. Vogel, M. Pakdel, M. Müller, H. Lindner, M.W. Hess, and D. Teis. 2014. Coordinated binding of Vps4 to ESCRT-III drives membrane neck constriction during MVB vesicle formation. *J. Cell Biol.* 205:33–49. http://dx.doi.org/10.1083/jcb.201310114

Ameen, N.A., and P.J. Salas. 2000. Microvillus inclusion disease: A genetic defect affecting apical membrane protein traffic in intestinal epithelium. *Traffic.* 1:76–83. http://dx.doi.org/10.1034/j.1600-0854.2000.010111.x

Apodaca, G., L.I. Gallo, and D.M. Bryant. 2012. Role of membrane traffic in the generation of epithelial cell asymmetry. *Nat. Cell Biol.* 14:1235–1243. http://dx.doi.org/10.1038/ncb2635

Baker, K.E., and R. Parker. 2004. Nonsense-mediated mRNA decay: Terminating erroneous gene expression. *Curr. Opin. Cell Biol.* 16:293–299. http://dx.doi.org/10.1016/j.ceb.2004.03.003

Bryant, D.M., A. Datta, A.E. Rodríguez-Fraticelli, J. Peränen, F. Martín-Belmonte, and K.E. Mostov. 2010. A molecular network for *de novo* generation of the apical surface and lumen. *Nat. Cell Biol.* 12:1035–1045. http://dx.doi.org/10.1038/ncb2106

Cartón-García, F., A.W. Overeem, R. Nieto, S. Bazzocco, H. Dopeso, I. Macaya, J. Bilic, S. Landolfi, J. Hernandez-Losa, S. Schwartz Jr., et al. 2015. *Myo5b* knockout mice as a model of microvillus inclusion disease. *Sci. Rep.* 5:12312. http://dx.doi.org/10.1038/srep12312

Chapin, H.C., and M.J. Caplan. 2010. The cell biology of polycystic kidney disease. *J. Cell Biol.* 191:701–710. http://dx.doi.org/10.1083/jcb.201006173

Chen, F., S.M. Pruett-Miller, Y. Huang, M. Gjoka, K. Duda, J. Taunton, T.N. Collingwood, M. Frodin, and G.D. Davis. 2011. High-frequency genome editing using ssDNA oligonucleotides with zinc-finger nucleases. *Nat. Methods.* 8:753–755. http://dx.doi.org/10.1038/nmeth.1653

Cutz, E., J.M. Rhoads, B. Drumm, P.M. Sherman, P.R. Durie, and G.G. Forstner. 1989. Microvillus inclusion disease: An inherited defect of brush-border assembly and differentiation. *N. Engl. J. Med.* 320:646–651. http://dx.doi.org/10.1056/NEJM198903093201006

Donovan, K.W., and A. Bretscher. 2012. Myosin-V is activated by binding secretory cargo and released in coordination with Rab/exocyst function. *Dev. Cell.* 23:769–781. http://dx.doi.org/10.1016/j.devcel.2012.09.001

Donovan, K.W., and A. Bretscher. 2015. Tracking individual secretory vesicles during exocytosis reveals an ordered and regulated process. *J. Cell Biol.* 210:181–189. http://dx.doi.org/10.1083/jcb.201501118

Duda, K., L.A. Lonowski, M. Kofoed-Nielsen, A. Ibarra, C.M. Delay, Q. Kang, Z. Yang, S.M. Pruett-Miller, E.P. Bennett, H.H. Wandall, et al. 2014. High-efficiency genome editing via 2A-coupled co-expression of fluorescent proteins and zinc finger nucleases or CRISPR/Cas9 nickase pairs. *Nucleic Acids Res.* 42:e84. http://dx.doi.org/10.1093/nar/gku251

Dukes, J.D., L. Fish, J.D. Richardson, E. Blaikley, S. Burns, C.J. Caunt, A.D. Chalmers, and P. Whitley. 2011. Functional ESCRT machinery is required for constitutive recycling of claudin-1 and maintenance of polarity in vertebrate epithelial cells. *Mol. Biol. Cell.* 22:3192–3205. http://dx.doi.org/10.1091/mbc.E11-04-0343

Fialka, I., C. Pasquali, F. Lottspeich, H. Ahorn, and L.A. Huber. 1997. Subcellular fractionation of polarized epithelial cells and identification of organelle-specific proteins by two-dimensional gel electrophoresis. *Electrophoresis.* 18:2582–2590. http://dx.doi.org/10.1002/elps.1150181414

Fukuda, M., A. Imai, T. Nashida, and H. Shimomura. 2005. Slp4-a/granuphilin-a interacts with syntaxin-2/3 in a Munc18-2-dependent manner. *J. Biol. Chem.* 280:39175–39184. http://dx.doi.org/10.1074/jbc.M505759200

Gaisano, H.Y., M. Ghai, P.N. Malkus, L. Sheu, A. Bouquillon, M.K. Bennett, and W.S. Trimble. 1996. Distinct cellular locations of the syntaxin family of proteins in rat pancreatic acinar cells. *Mol. Biol. Cell.* 7:2019–2027. http://dx.doi.org/10.1091/mbc.7.12.2019

Galli, T., A. Zahraoui, V.V. Vaidyanathan, G. Raposo, J.M. Tian, M. Karin, H. Niemann, and D. Louvard. 1998. A novel tetanus neurotoxin-insensitive vesicle-associated membrane protein in SNARE complexes of the apical plasma membrane of epithelial cells. *Mol. Biol. Cell.* 9:1437–1448. http://dx.doi.org/10.1091/mbc.9.6.1437

Gálvez-Santisteban, M., A.E. Rodriguez-Fraticelli, D.M. Bryant, S. Vergarajauregui, T. Yasuda, I. Bañón-Rodríguez, I. Bernascone, A. Datta, N. Spivak, K. Young, et al. 2012. Synaptotagmin-like proteins control the formation of a single apical membrane domain in epithelial cells. *Nat. Cell Biol.* 14:838–849. http://dx.doi.org/10.1038/ncb2541

Glatter, T., A. Wepf, R. Aebersold, and M. Gstaiger. 2009. An integrated workflow for charting the human interaction proteome: Insights into the PP2A system. *Mol. Syst. Biol.* 5:237. http://dx.doi.org/10.1038/msb.2008.75

Holubcová, Z., G. Howard, and M. Schuh. 2013. Vesicles modulate an actin network for asymmetric spindle positioning. *Nat. Cell Biol.* 15:937–947. http://dx.doi.org/10.1038/ncb2802

Hsu, P.D., D.A. Scott, J.A. Weinstein, F.A. Ran, S. Konermann, V. Agarwala, Y. Li, E.J. Fine, X. Wu, O. Shalem, et al. 2013. DNA targeting specificity of RNA-guided Cas9 nucleases. *Nat. Biotechnol.* 31:827–832. http://dx.doi.org/10.1038/nbt.2647

Huber, L.A., S. Pimplikar, R.G. Parton, H. Virta, M. Zerial, and K. Simons. 1993. Rab8, a small GTPase involved in vesicular traffic between the TGN and

the basolateral plasma membrane. *J. Cell Biol.* 123:35–45. http://dx.doi.org/10.1083/jcb.123.1.35

Iancu, T.C., M. Mahajnah, I. Manov, and R. Shaoul. 2007. Microvillous inclusion disease: Ultrastructural variability. *Ultrastruct. Pathol.* 31:173–188. http://dx.doi.org/10.1080/01913120701350712

Jaffe, A.B., N. Kaji, J. Durgan, and A. Hall. 2008. Cdc42 controls spindle orientation to position the apical surface during epithelial morphogenesis. *J. Cell Biol.* 183:625–633. http://dx.doi.org/10.1083/jcb.200807121

Jin, Y., A. Sultana, P. Gandhi, E. Franklin, S. Hamamoto, A.R. Khan, M. Munson, R. Schekman, and L.S. Weisman. 2011. Myosin V transports secretory vesicles via a Rab GTPase cascade and interaction with the exocyst complex. *Dev. Cell.* 21:1156–1170. http://dx.doi.org/10.1016/j.devcel.2011.10.009

Khandelwal, P., H.S. Prakasam, D.R. Clayton, W.G. Ruiz, L.I. Gallo, D. van Roekel, S. Lukianov, J. Peränen, J.R. Goldenring, and G. Apodaca. 2013. A Rab11a-Rab8a-Myo5B network promotes stretch-regulated exocytosis in bladder umbrella cells. *Mol. Biol. Cell.* 24:1007–1019. http://dx.doi.org/10.1091/mbc.E12-08-0568

Knowles, B.C., J.T. Roland, M. Krishnan, M.J. Tyska, L.A. Lapierre, P.S. Dickman, J.R. Goldenring, and M.D. Shub. 2014. Myosin Vb uncoupling from RAB8A and RAB11A elicits microvillus inclusion disease. *J. Clin. Invest.* 124:2947–2962. http://dx.doi.org/10.1172/JCI71651

Knowles, B.C., V.G. Weis, S. Yu, J.T. Roland, J.A. Williams, G.S. Alvarado, L.A. Lapierre, M.D. Shub, N. Gao, and J.R. Goldenring. 2015. Rab11a regulates syntaxin 3 localization and microvillus assembly in enterocytes. *J. Cell Sci.* 128:1617–1626. http://dx.doi.org/10.1242/jcs.163303

Kremer, J.R., D.N. Mastronarde, and J.R. McIntosh. 1996. Computer visualization of three-dimensional image data using IMOD. *J. Struct. Biol.* 116:71–76. http://dx.doi.org/10.1006/jsbi.1996.0013

Lapierre, L.A., M.C. Dorn, C.F. Zimmerman, J. Navarre, J.O. Burnette, and J.R. Goldenring. 2003. Rab11b resides in a vesicular compartment distinct from Rab11a in parietal cells and other epithelial cells. *Exp. Cell Res.* 290:322–331. http://dx.doi.org/10.1016/S0014-4827(03)00340-9

Larmonier, C.B., D. Laubitz, F.M. Hill, K.W. Shehab, L. Lipinski, M.T. Midura-Kiela, R.M. McFadden, R. Ramalingam, K.A. Hassan, M. Golebiewski, et al. 2013. Reduced colonic microbial diversity is associated with colitis in NHE3-deficient mice. *Am. J. Physiol. Gastrointest. Liver Physiol.* 305:G667–G677. http://dx.doi.org/10.1152/ajpgi.00189.2013

Li, X., S.H. Low, M. Miura, and T. Weimbs. 2002. SNARE expression and localization in renal epithelial cells suggest mechanism for variability of trafficking phenotypes. *Am. J. Physiol. Renal Physiol.* 283:F1111–F1122. http://dx.doi.org/10.1152/ajprenal.00185.2002

Lim, Y.S., and B.L. Tang. 2013. The Evi5 family in cellular physiology and pathology. *FEBS Lett.* 587:1703–1710. http://dx.doi.org/10.1016/j.febslet.2013.04.036

Low, S.H., S.J. Chapin, T. Weimbs, L.G. Kömüves, M.K. Bennett, and K.E. Mostov. 1996. Differential localization of syntaxin isoforms in polarized Madin-Darby canine kidney cells. *Mol. Biol. Cell.* 7:2007–2018. http://dx.doi.org/10.1091/mbc.7.12.2007

Martin-Belmonte, F., A. Gassama, A. Datta, W. Yu, U. Rescher, V. Gerke, and K. Mostov. 2007. PTEN-mediated apical segregation of phosphoinositides controls epithelial morphogenesis through Cdc42. *Cell.* 128:383–397. http://dx.doi.org/10.1016/j.cell.2006.11.051

Moyer, B.D., J. Denton, K.H. Karlson, D. Reynolds, S. Wang, J.E. Mickle, M. Milewski, G.R. Cutting, W.B. Guggino, M. Li, and B.A. Stanton. 1999. A PDZ-interacting domain in CFTR is an apical membrane polarization signal. *J. Clin. Invest.* 104:1353–1361. http://dx.doi.org/10.1172/JCI7453

Müller, T., M.W. Hess, N. Schiefermeier, K. Pfaller, H.L. Ebner, P. Heinz-Erian, H. Ponstingl, J. Partsch, B. Röllinghoff, H. Köhler, et al. 2008. *MYO5B* mutations cause microvillus inclusion disease and disrupt epithelial cell polarity. *Nat. Genet.* 40:1163–1165. http://dx.doi.org/10.1038/ng.225

Overeem, A.W., D.M. Bryant, and S.C. van IJzendoorn. 2015. Mechanisms of apical-basal axis orientation and epithelial lumen positioning. *Trends Cell Biol.* 25:476–485. http://dx.doi.org/10.1016/j.tcb.2015.04.002

Paulick, M.G., and C.R. Bertozzi. 2008. The glycosylphosphatidylinositol anchor: A complex membrane-anchoring structure for proteins. *Biochemistry.* 47:6991–7000. http://dx.doi.org/10.1021/bi8006324

Peränen, J., P. Auvinen, H. Virta, R. Wepf, and K. Simons. 1996. Rab8 promotes polarized membrane transport through reorganization of actin and microtubules in fibroblasts. *J. Cell Biol.* 135:153–167. http://dx.doi.org/10.1083/jcb.135.1.153

Phillips, A., J. Fransen, H.P. Hauri, and E. Sterchi. 1993. The constitutive exocytotic pathway in microvillous atrophy. *J. Pediatr. Gastroenterol. Nutr.* 17:239–246. http://dx.doi.org/10.1097/00005176-199310000-00002

Phillips, A.D., M. Szafranski, L.Y. Man, and W.J. Wall. 2000. Periodic acid-Schiff staining abnormality in microvillous atrophy: Photometric and ultrastructural studies. *J. Pediatr. Gastroenterol. Nutr.* 30:34–42. http://dx.doi.org/10.1097/00005176-200001000-00015

Pocard, T., A. Le Bivic, T. Galli, and C. Zurzolo. 2007. Distinct v-SNAREs regulate direct and indirect apical delivery in polarized epithelial cells. *J. Cell Sci.* 120:3309–3320. http://dx.doi.org/10.1242/jcs.007948

Provance, D.W. Jr., E.J. Addison, P.R. Wood, D.Z. Chen, C.M. Silan, and J.A. Mercer. 2008. Myosin-Vb functions as a dynamic tether for peripheral endocytic compartments during transferrin trafficking. *BMC Cell Biol.* 9:44. http://dx.doi.org/10.1186/1471-2121-9-44

Pylypenko, O., W. Attanda, C. Gauquelin, M. Lahmani, D. Coulibaly, B. Baron, S. Hoos, M.A. Titus, P. England, and A.M. Houdusse. 2013. Structural basis of myosin V Rab GTPase-dependent cargo recognition. *Proc. Natl. Acad. Sci. USA.* 110:20443–20448. http://dx.doi.org/10.1073/pnas.1314329110

Reinshagen, K., H.Y. Naim, and K.P. Zimmer. 2002. Autophagocytosis of the apical membrane in microvillus inclusion disease. *Gut.* 51:514–521. http://dx.doi.org/10.1136/gut.51.4.514

Rodriguez-Boulan, E., and I.G. Macara. 2014. Organization and execution of the epithelial polarity programme. *Nat. Rev. Mol. Cell Biol.* 15:225–242. http://dx.doi.org/10.1038/nrm3775

Roland, J.T., L.A. Lapierre, and J.R. Goldenring. 2009. Alternative splicing in class V myosins determines association with Rab10. *J. Biol. Chem.* 284:1213–1223. http://dx.doi.org/10.1074/jbc.M805957200

Roland, J.T., D.M. Bryant, A. Datta, A. Itzen, K.E. Mostov, and J.R. Goldenring. 2011. Rab GTPase-Myo5B complexes control membrane recycling and epithelial polarization. *Proc. Natl. Acad. Sci. USA.* 108:2789–2794. http://dx.doi.org/10.1073/pnas.1010754108

Ruemmele, F.M., J. Schmitz, and O. Goulet. 2006. Microvillous inclusion disease (microvillous atrophy). *Orphanet J. Rare Dis.* 1:22. http://dx.doi.org/10.1186/1750-1172-1-22

Ruemmele, F.M., T. Müller, N. Schiefermeier, H.L. Ebner, S. Lechner, K. Pfaller, C.E. Thöni, O. Goulet, F. Lacaille, J. Schmitz, et al. 2010. Loss-of-function of MYO5B is the main cause of microvillus inclusion disease: 15 novel mutations and a CaCo-2 RNAi cell model. *Hum. Mutat.* 31:544–551. http://dx.doi.org/10.1002/humu.21224

Salomon, J., O. Goulet, D. Canioni, N. Brousse, J. Lemale, P. Tounian, A. Coulomb, E. Marinier, J.P. Hugot, F. Ruemmele, et al. 2014. Genetic characterization of congenital tufting enteropathy: epcam associated phenotype and involvement of SPINT2 in the syndromic form. *Hum. Genet.* 133:299–310. http://dx.doi.org/10.1007/s00439-013-1380-6

Sanjana, N.E., O. Shalem, and F. Zhang. 2014. Improved vectors and genome-wide libraries for CRISPR screening. *Nat. Methods.* 11:783–784. http://dx.doi.org/10.1038/nmeth.3047

Sato, T., S. Mushiake, Y. Kato, K. Sato, M. Sato, N. Takeda, K. Ozono, K. Miki, Y. Kubo, A. Tsuji, et al. 2007. The Rab8 GTPase regulates apical protein localization in intestinal cells. *Nature.* 448:366–369. http://dx.doi.org/10.1038/nature05929

Schmidt, T.G., and A. Skerra. 2007. The Strep-tag system for one-step purification and high-affinity detection or capturing of proteins. *Nat. Protoc.* 2:1528–1535. http://dx.doi.org/10.1038/nprot.2007.209

Schneeberger, K., G.F. Vogel, H. Teunissen, D.D. van Ommen, H. Begthel, L. El Bouazzaoui, A.H.M. van Vugt, J.M. Beekman, J. Klumperman, T. Müller, et al. 2015. An inducible mouse model for microvillus inclusion disease reveals a role for myosin Vb in apical and basolateral trafficking. *Proc. Natl. Acad. Sci. USA.* 112:12408–12413. http://dx.doi.org/10.1073/pnas.1516672112

Schuh, M. 2011. An actin-dependent mechanism for long-range vesicle transport. *Nat. Cell Biol.* 13:1431–1436. http://dx.doi.org/10.1038/ncb2353

Sigl, R., C. Ploner, G. Shivalingaiah, R. Kofler, and S. Geley. 2014. Development of a multipurpose GATEWAY-based lentiviral tetracycline-regulated conditional RNAi system (GLTR). *PLoS One.* 9:e97764. http://dx.doi.org/10.1371/journal.pone.0097764

Sobajima, T., S. Yoshimura, T. Iwano, M. Kunii, M. Watanabe, N. Atik, S. Mushiake, E. Morii, Y. Koyama, E. Miyoshi, and A. Harada. 2014. Rab11a is required for apical protein localisation in the intestine. *Biol. Open.* 4:86–94. http://dx.doi.org/10.1242/bio.20148532

Swiatecka-Urban, A., L. Talebian, E. Kanno, S. Moreau-Marquis, B. Coutermarsh, K. Hansen, K.H. Karlson, R. Barnaby, R.E. Cheney, G.M. Langford, et al. 2007. Myosin Vb is required for trafficking of the cystic fibrosis transmembrane conductance regulator in Rab11a-specific apical recycling endosomes in polarized human airway epithelial cells. *J. Biol. Chem.* 282:23725–23736. http://dx.doi.org/10.1074/jbc.M608531200

Tang, B.L., H.Y. Gee, and M.G. Lee. 2011. The cystic fibrosis transmembrane conductance regulator's expanding SNARE interactome. *Traffic.* 12:364–371. http://dx.doi.org/10.1111/j.1600-0854.2011.01161.x

Thoeni, C.E., G.F. Vogel, I. Tancevski, S. Geley, S. Lechner, K. Pfaller, M.W. Hess, T. Müller, A.R. Janecke, Y. Avitzur, et al. 2014. Microvillus

inclusion disease: Loss of Myosin vb disrupts intracellular traffic and cell polarity. *Traffic.* 15:22–42. http://dx.doi.org/10.1111/tra.12131

Uldry, M., and B. Thorens. 2004. The SLC2 family of facilitated hexose and polyol transporters. *Pflugers Arch.* 447:480–489. http://dx.doi.org/10.1007/s00424-003-1085-0

Ullrich, O., S. Reinsch, S. Urbé, M. Zerial, and R.G. Parton. 1996. Rab11 regulates recycling through the pericentriolar recycling endosome. *J. Cell Biol.* 135:913–924. http://dx.doi.org/10.1083/jcb.135.4.913

van der Velde, K.J., H.S. Dhekne, M.A. Swertz, S. Sirigu, V. Ropars, P.C. Vinke, T. Rengaw, P.C. van den Akker, E.H. Rings, A. Houdusse, and S.C. van Ijzendoorn. 2013. An overview and online registry of microvillus inclusion disease patients and their MYO5B mutations. *Hum. Mutat.* 34:1597–1605. http://dx.doi.org/10.1002/humu.22440

Vogel, G.F., H.L. Ebner, M.E.G. de Araujo, T. Schmiedinger, O. Eiter, H. Pircher, K. Gutleben, B. Witting, D. Teis, L.A. Huber, and M.W. Hess. 2015. Ultrastructural morphometry points to a new role for LAMTOR2 in regulating the endo/lysosomal system. *Traffic.* 16:617–634. http://dx.doi.org/10.1111/tra.12271

Wang, C.C., H. Shi, K. Guo, C.P. Ng, J. Li, B.Q. Gan, H. Chien Liew, J. Leinonen, H. Rajaniemi, Z.H. Zhou, et al. 2007. VAMP8/endobrevin as a general vesicular SNARE for regulated exocytosis of the exocrine system. *Mol. Biol. Cell.* 18:1056–1063. http://dx.doi.org/10.1091/mbc.E06-10-0974

Weimbs, T., S.H. Low, S.J. Chapin, and K.E. Mostov. 1997. Apical targeting in polarized epithelial cells: There's more afloat than rafts. *Trends Cell Biol.* 7:393–399. http://dx.doi.org/10.1016/S0962-8924(97)01130-6

Weinman, E.J., Y. Wang, F. Wang, C. Greer, D. Steplock, and S. Shenolikar. 2003. A C-terminal PDZ motif in NHE3 binds NHERF-1 and enhances cAMP inhibition of sodium–hydrogen exchange. *Biochemistry.* 42:12662–12668. http://dx.doi.org/10.1021/bi035244l

Weisz, O.A., and E. Rodriguez-Boulan. 2009. Apical trafficking in epithelial cells: Signals, clusters and motors. *J. Cell Sci.* 122:4253–4266. http://dx.doi.org/10.1242/jcs.032615

Westlake, C.J., L.M. Baye, M.V. Nachury, K.J. Wright, K.E. Ervin, L. Phu, C. Chalouni, J.S. Beck, D.S. Kirkpatrick, D.C. Slusarski, et al. 2011. Primary cilia membrane assembly is initiated by Rab11 and transport protein particle II (TRAPPII) complex-dependent trafficking of Rabin8 to the centrosome. *Proc. Natl. Acad. Sci. USA.* 108:2759–2764. http://dx.doi.org/10.1073/pnas.1018823108

Wiegerinck, C.L., A.R. Janecke, K. Schneeberger, G.F. Vogel, D.Y. van Haaften-Visser, J.C. Escher, R. Adam, C.E. Thöni, K. Pfaller, A.J. Jordan, et al. 2014. Loss of syntaxin 3 causes variant microvillus inclusion disease. *Gastroenterology.* 147:65–68.e10. http://dx.doi.org/10.1053/j.gastro.2014.04.002

Yang, J., X. Zhao, A. Patel, R. Potru, S. Azizi-Ghannad, M. Dolinger, J. Cao, C. Bartholomew, J. Mazurkiewicz, D. Conti, et al. 2015. Rapamycin inhibition of mTOR reduces levels of the Na^+/H^+ Exchanger 3 in intestines of mice and humans, leading to diarrhea. *Gastroenterology.* 149:151–162. http://dx.doi.org/10.1053/j.gastro.2015.03.046

Yoo, B.K., M.K. Yanda, Y.R. No, and C.C. Yun. 2012. Human intestinal epithelial cell line SK-CO15 is a new model system to study Na^+/H^+ exchanger 3. *Am. J. Physiol. Gastrointest. Liver Physiol.* 303:G180–G188. http://dx.doi.org/10.1152/ajpgi.00069.2012

Yoshimura, S., J. Egerer, E. Fuchs, A.K. Haas, and F.A. Barr. 2007. Functional dissection of Rab GTPases involved in primary cilium formation. *J. Cell Biol.* 178:363–369. http://dx.doi.org/10.1083/jcb.200703047